Analytical Optimization of X-ray Mammography Technique for Increased Benefits and Safety; using: Data Analytics, Electronics Engineering and Artificial Intelligence[1]

Chikezie Kennedy Kalu
Department of Management Science and Engineering,
School of Management; Jiangsu University,
301 Xuefu Road, Zhenjiang, Jiangsu Province/China
53 Omu-Aran Street; Unity Estate, Egbeda. Lagos/Nigeria

Abstract

To understand, analyse, and investigate common X-ray Mammography techniques, terminologies and properties; and how the X-ray Mammography systems can be optimized for a safer, more effective, more efficient, more energy efficient procedure for breast cancer diagnosis; using Deep Learning (DL)/Artificial Intelligence (AI) , Analytical, Electronic Engineering, tools and Methodologies. Using data and breast cancer image datasets from validated open source data stores; investigative and comparative analyses were carried out on common X-ray Mammography techniques in relation to breast cancer diagnosis and treatments, as well as optimization analyses using Electronic engineering principles and Artificial Intelligence principles on the quality, intensity, X-ray Mammography properties, processes and system. The methodical and data-driven analyses were carried out using the following Data, Artificial Intelligence (AI) and Electronic Engineering, methodologies and

[1] **FUNDING:** I am currently on a PhD Scholarship from the Chinese Government. No specific finding for this Research work.

algorithms: Data Analytics, Convolutional Neural Networks (CNN) in Machine Learning (ML) Engineering, and X-ray-Impedance Circuit Composite System Analysis. The modern CESM (Contrast-Enhanced Spectral Mammography) technique, confirms to be the most efficient especially for a dense breast, but other techniques (including CESM) can also improve in efficiency when set up with the appropriate metal filter combination(s). Furthermore, the electronic impedance circuit shows good promise in the intelligent reduction of X-ray radiation intensity and further variations in energy; which is needed for a safer and quality X-ray Mammography procedure. Additionally, an interesting estimation of the number of pooling layers needed to achieve a quality metric for breast cancer image classification was investigated and proposed.

Data, AI and Technological processes, techniques and systems are shown to be a promising contributor to medical science; and will no doubt create huge collaborative and multidisciplinary solutions needed for more efficient, effective and safer diagnoses and treatments of breast cancer and also potentially other forms of cancer.

Keywords: X-ray Mammography, Breast Cancer, Women, Data, Analytics, Convolutional Neural Networks (CNN), Artificial Intelligence, Electronic Impedance Circuit, Medical Imaging, Electronics Engineering.

1. INTRODUCTION

The most common and fatal cancers amongst women is breast cancer. Between 2016 to 2020 alone, official reports from the World Health Organisation (WHO) indicates approximately 7.8 million cases of breast cancer, of which 685,000 of them have died (Enshafi et al. 2022), which makes it a serious killer of an ailment. For easier treatment of breast cancer and also the accompanying reduction of the mortality rate caused by the disease; early detection is pertinent and must be continually optimized to fight the disease effectively and efficiently (Mashekova et al. 2022:27). It is therefore recommended for women aged between 40 to 75

years old have periodic breast screening, because early breast diagnosis and treatment of breast lesions, as shown by facts, can be achieved by breast screening performed by using different X-ray imaging techniques (Chamieh et al. 2022:22). Most Cancers in general can be benign or malignant, depending on its nature and form of spread. The malignant cancer lesions consumes on the nutrients of other tissues and spreads throughout the body, while the benign cancer lesions, do not affect the surrounding tissues, but stay lumped around a specific area (Mahmood et al., 2020). Compared to other medical procedures, mammography is considered the most preferred method for screening breast cancer (Sutton,1998).

However, the risk and continuous exposure to harmful radiation is associated with frequent medical screenings for cancer, especially for the widely used annual mammograms to detect breast cancer (Rashid et al. 2021). A previous study indicates that the radiation dose per mammography procedure is around 3.0 mSv (Shields & Wilkins, 2009). The mostly used two-dimensional mammograms from different projections, takes X-ray images of each breast as a standard procedure. The three primary regions of the female breast are (1) The skin region, (2) the subcutaneous adipose tissue just beneath the skin and (3) the mixed adipose and glandular tissue, of which the average dose absorbed is called the average glandular dose(AGD) (Schapira , Clark , Wolff , Jarrett , Kumar , Aziz, 1994; Shuster, Patlas, Pinthus, Mourtzakis, 2012). To also ensure the safety of X-ray procedures with respect to acceptable radiation levels; agencies like the International Commission on Radiological Protection and the Institute of Medicine have promulgated recommended AGD levels (Valentin, 2007).

Therefore, optimizing X-ray Mammography procedures, to deliver even better quality screening, and still operate at a safe level of radiation and radiation intensity is a continual urgent need towards the effective and efficient diagnosis, prevention, treatments and management of breast cancer. Additionally, a modern reasonable assessment of the quality of the mammogram should be in its ability to compulsorily strike a balance between benefits and risks of patients exposure (Saeed, 2021). For a data-driven world of ours, and the huge opportunities presented by Data, AI, digital healthcare and associated technologies; innovative measures to analyse, manage and optimize X-ray Mammography procedures have great potentials to improve screening procedures, reduce mortality rates and provide continuous improvements to systems for the diagnosis, treatment and management of breast cancer, in

safer, more precise and less risky approaches. With also the current advancements in imaging techniques, further multidisciplinary collaborations and use of technologies, increased knowledge sharing and awareness creation about breast cancer, will further excellently position the healthcare system to tackle cancer cases even more comprehensively.

The aim of this research work is to understand and investigate common X-ray Mammography techniques, terminologies and properties; and how the X-ray Mammography systems can be optimized for a safer, more effective, more efficient, more energy efficient procedure for breast cancer diagnosis; thereby aiding medical personnel, researchers, processes, policy decision makers to effectively and efficiently tackle breast cancer cases and improve the lives of women and humanity; with the use of modern Data, AI and technological tools.

2. LITERATURE REVIEW

2.1 X-ray Mammography For Breast Cancer

Mortality rate of breast cancer has been shown to be reduced by screening mammography, which detects breast cancer early (James, 2017). Mammography is usually considered the standard for breast cancer screening, but factors such as dense breast tissue may affect the imaging sensitivity and specificity. The cost of false positive findings is large, as a recent study noted that false-positive diagnostic mammography cost 2.8billion ndollars per year as noted by a report conducted for about 3.2million Ameriacn women (Pisano, Gatsonis, Hendrick, et al., 2005; Carbonaro, Di Leo, Clauser et al., 2016). Therefore, to improve patient care and overall cancer quality detection, more advancement in imaging techniques such as 3D tomosynthesis, contrast-enhanced spectral mammography (CESM), molecular breast imaging, breast MRI, and others; are used to reduce false-positive rates without compromising sensitivity and safety for patients (Cheung, Lin, Wan, et al., 2014; Haas, Kalra, Geisel, Raghu, Durand, Philpotts, 2013; Luczyńska, Heinze-Paluchowska, Hendrick, et al. 2015; Holbrook, Newel, 2015; MK, 2015; Mori, Akashi-Tanaka, Suzuki, et al. 2016) With the advantage of the combination of standard full field digital mammography (FFDM) with contrast-enhanced high and low energy images; the CESM is a novel breast imaging technique.

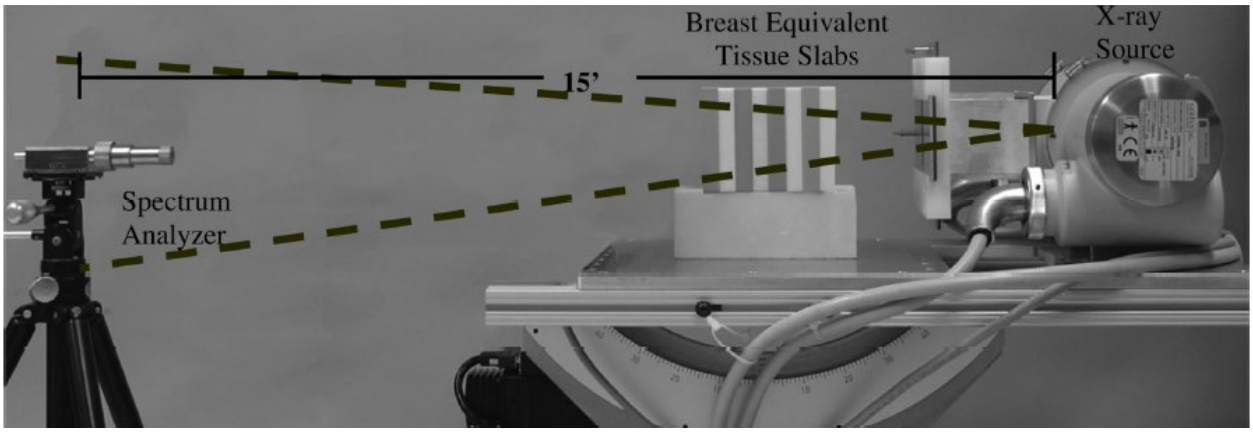

Figure 1: Experimental setup showing the x-ray source and partially collimated cone beam passing through slabs of breast equivalent tissue (resting on styrofoam) towards the spectrum analyser. Note that the actual separation between the x-ray source focal spot and detector window is approximately 15 ft in order to reduce flux. For several measurements, the breast slabs were removed. Note that the image is not to scale (Crotty et al., 2012)

Also, other new techniques, like the Dual energy mammography technique, leads to the enhancement of pathogegenesis not present in screening mammography, by suppressing the contrast between adipose and glandular tissues (Taibi, Vecchio, 2014). Previous studies also indicate that adopting the dual energy technique is very promising, as results shows improvements regardless of the method used to obtain the dual energy image (Martini et al., 2020). Furthermore, the indication of malignancy and disease state may be made by the type of calcification crystals present in a mammogram, according to several studies (Wu, Chiang, Zhou, 2017; Han et al., 2020; Fandos-Morera et al., 1988). For example, both minimum and microcalcification size or thickness, detection and visualization were explored by the analytical model developed band used in simulation studies conducted (Lemacks et al., 2002; Brandan & Ramirez, 2006; Koukou et al., 2015; Del Lama et al., 2017). An important demographic marker used in screening risk for breast cancer is the radiographic density of the breast. Classification of breast types are originally based on their radio-opacity obtained from x-ray mammograms which are determined from parenchymal patterns (Boyd et al., 2001).

Amongst the various types of mammography, which includes film mammography, digital mammography, etc; the digital mammography possess a higher cancer detection rate than the film mammography. Detecting and guiding cancer treatments, are the main aim of

mammography (Khalkhali et al., 1994; Heywang-Köbrunner et al., 2011; Ramani & Suthanthira, 2014) as also depicted in Figure 1, and it is a well established and cost effective breast detection imaging technique (Duffy, 2006; Taba, Yen, Vitak et al., 2003; Otto, Fracheboud, Looman et al., 2003). Though with regular progress, conventional mammography and full-field digital mammography have limitations, particularly in treated and dense breasts (Rosenber, Hunt, Williamson et al., 1998).

2.2 Convolutional Neural Networks (CNN) for breast cancer screening

CNN has become the most popular algorithm to build efficient models in the world of image classification. CNN's are similar to ordinary neural networks, except that it explicitly assumes that the inputs are images, which allows us to encode certain properties into the architecture. This then ensures the parameters in the network are reduced and thereby makes the forward function more efficient to implement. The neurons are arranged in three dimensions: width, height, and depth. Generally, as also shown in Figure 2, CNN consists of four main types of layers: input layer, convolution layer, pooling layer, fully connected layer (Swamynathan, 2017).

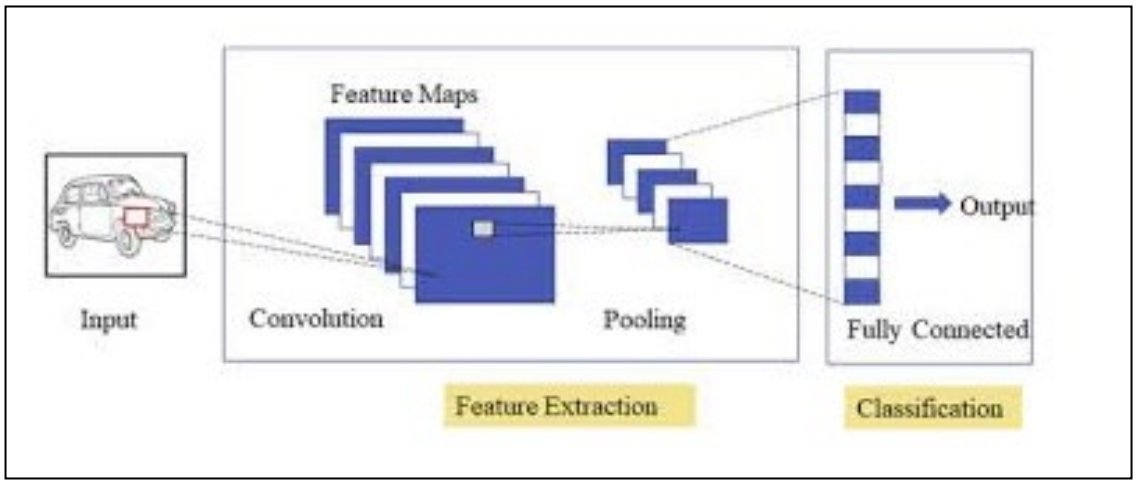

Figure 2: CNN Systems Description for Image Classification (Source : Google Images)

Opportunities have opened up on addressing the challenge of using Deep Learning(DL) methods for early detection of breast cancer, by the significant progress in machine learning and techniques of image processing, and prevalence of digital MG(mammogram) images due to the recent advances in computational technologies (LeCun, Bengio, 2015; Litjens, Kooi, Bejnordi, Setio, Ciompi, Ghafoorian, et al., 2017; Zhao et al., 2016; Lee et al., 2017). CAD

(Computer Aided Design) systems' limitations, have been overcome by the help of the recent Deep learning method: CNN (also known as ConvNets), which has gained lots of attention to CAD (Li, Chen, Cao, Ma, 2016; Hedjazi, Kourbane, Genc, 2017). CNNs help radiologists with more accurate diagnosis, achieving higher detection accuracy than CAD models, and delivering quantitative analysis of suspicious lesions. With higher precision and processing ability, current CNN models are designed to improve radiologists' ability to find even the smallest breast cancers at their earliest stages alerting the radiologist to the need for further analysis and further research study shows that human error rate for breast cancer diagnoses drop by 85%, when using DL methods (Kooi, Gubern-Merida, Mordang, Mann, Pijnappel, Schuur, et al., 2016; Chartrand, Cheng, Vorontsov, Drozdzal, Turcotte, Pal, et al., 2017; Platania et al., 2017; Wang et al., 2017) .

A lot of breakthroughs in a variety of pattern recognition and classification problems have been let by CNNs in the last few years. Also, breakthroughs using CNN for natural images have been aided by the availability of big data repositories, fast graphical processing units and power of parallel and distributed computing (Krizhevsky, Sutskever, Hinton, 2012; Greenspan, van Ginneken, Summers, 2016). When working with a limited number of medical data, training a deep learning CNN model can be very challenging, and such can be addressed by using transfer learning(TL) and augmentation techniques (Weiss, Khoshgoftaar, Wang, 2016). Studies show that CNN methods that compare images from left and right breasts (Christoyianni, Constantinou, Dermatas, 2004) and also the craniocaudal (CC) and mediolateral-oblique (MLO) view of each breast can improve the accuracy of detection and reduce the false positives (Zhu, Lou, Vang, Xie, 2017; Kooi, Ginneken, Karssemeijer, Heeten, 2017; Geras, Wolfson, Kim, Moy, Cho, 2017; Yi, Sawyer, Cohn, Dunnmon, Lam, Xiao et al., 2017; Ben-Ari, Akselrod-Ballin, Karlinsky, Hashoul, 2017; (Dhungel, Carneiro, Bradley, 2017) . CNNs have been employed by radiologists to increase the accuracy of early detection of breast cancer by carrying out the required risk assessment applications (Fonseca, Mendoza, Wainer, Ferrer, Pinto, Guerrero et al., 2015; Kallenberg, Petersen, Nielsen, Ng, Diao, Igel et al., 2016; Oustimov , Gastounioti, Hsieh, Pantalone, Conant, Kontos, 2017; Petersen, Nielsen, Diao, Karssemeijer, Lillholm, 2014; Qiu, Wang, Yan, Tan, Cheng, Liu et al., 2016; Sun, Tseng,

Zheng, Qian, 2016; Carneiro, Nascimento, Bradley, 2015; Becker, Marcon, Ghafoor, Wurnig, Frauenfelder, Boss, 2017; Ahn, Heo, Ji, Kim, 2017; Li, Giger, Huynh, 2017).

3. METHODOLOGY

This research activity and study is very much data driven, as it involves the synthesis of X-ray Mammography techniques, X-ray Mammography terminologies, X-ray Mammography properties, Deep Learning or Artificial Intelligence Convolutional Neural Network(CNN) data; relating to breast cancer diagnosis and treatments and relevant to the literature from diverse databases and portals. The set analyses were carried out in two broad sections of Analysis of X-ray Mammography Techniques and properties for breast Cancer and then Image Classification using Artificial Intelligence CNN algorithms respectively that influences breast cancer treatments and the optimization (medical and energy) of such processes. The research activities revolved around the various data analysis, data analytics, Electronic Engineering principles and theories; and CNN processes to carry out the necessary studies and obtain results. In addition to the theoretical and practical concepts and parameters already known; new metrics are derived to indicate, measure and confirm key tests and analyses.

3.1. Data Collection and Preparation

Furthermore, for such various methodical analyses; data acquisition, data cleaning, data wrangling, image datasets preprocessing, sizing and cropping; are among key preliminary steps to ensure that the required data is importantly used for such analysis, following the key important steps:

- Step 1 : Acquire data from validated open access data stores and live data web portals
- Step 2 : Clean the data, label it appropritely, process it, wrangle it and make it fit for purpose
- Step 3: Store the data and partition them accordingly for use
- Step 4 : Feed the data into the particular analysis tool, model and process as required.
- Step 5 : Prepare and specify how results will be reported

3.2. Research Process Flow

The research activity carried out in addition to data acquisition and associated process, is summarized by the flowchart in Figure 3.

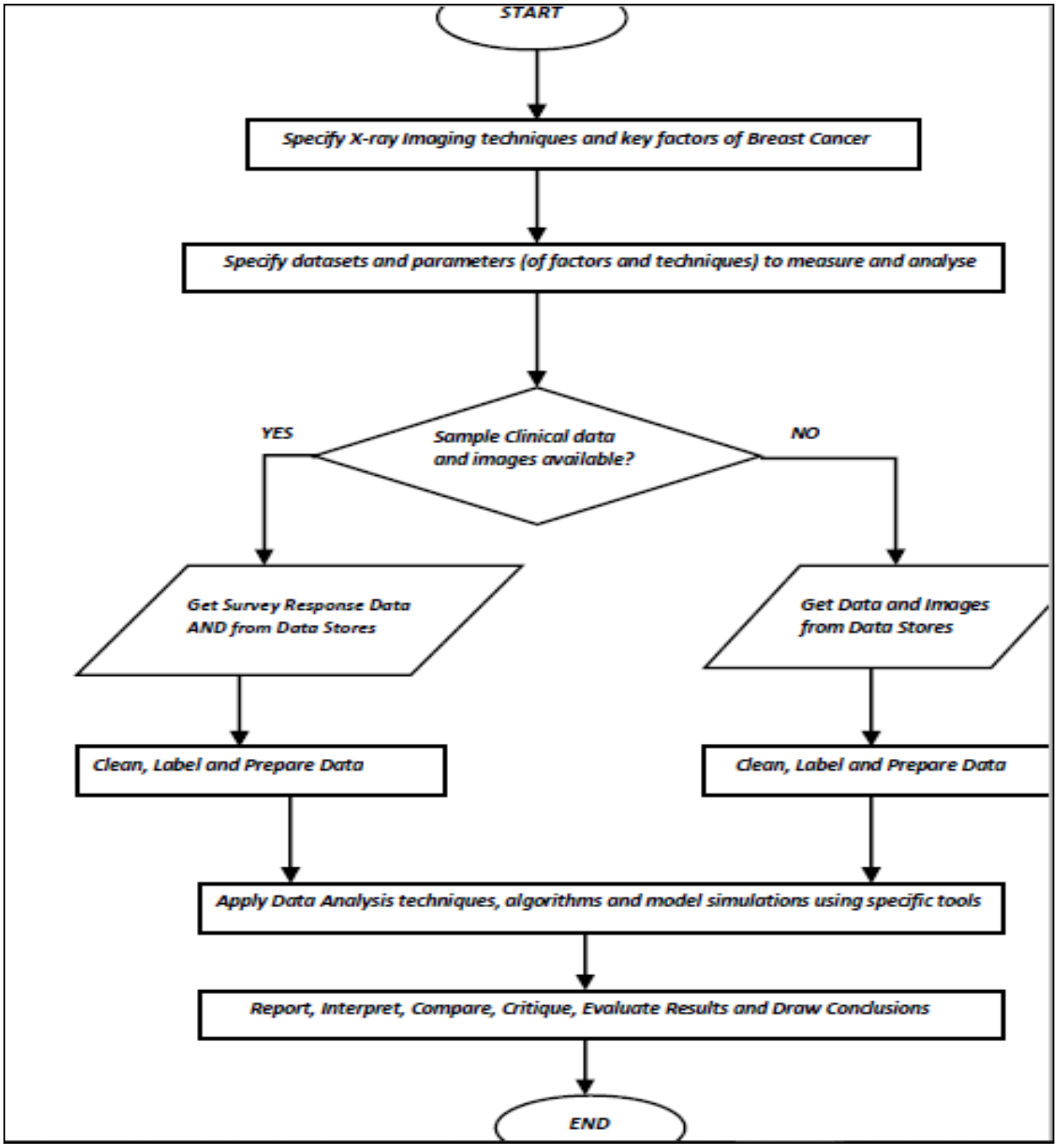

Figure 3: Summarized Research Process Flowchart

3.3 Analytical Optimization of X-ray procedure using electronic impedance Circuit

For this analytical mathematical approach to the optimization of X-ray procedure from an intensity point of view, as it relates with breast cancer; the focus is to be able to intelligently reduce the intensity of an X-ray beam to the human tissue using electronic impedance circuit, thereby making the procedure safer and more energy efficient, by also providing extra room for X-rays to utilize more energy with lesser intensity and better/optimal quality of diagnosis. The system conceptual model and analytical background are described:

3.3.1 System Conceptual Model

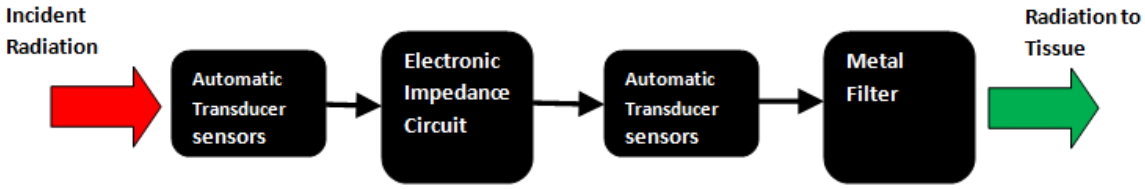

Figure 4: System description of X-ray Impedance Circuit

Composite System for mammography

Generally, as depicted in Figure 4, the incident radiation from the X-ray mammogram source is converted to electrical energy by the first set of input automatics transducer sensors; and then this electrical signal is then processed by the bank of impedances in the electronics circuit and the intensity or energy of the signal is adjusted accordingly. This adjusted signal intensity is then fed to the output automatic transducer sensors which then reconvert the electrical signal to its equivalent radiation signal, which is then received by the metal filter, which then uses its inherent properties to feed the appropriate radiation amount to the human body tissue or breast.

3.3.2 Analytical Description

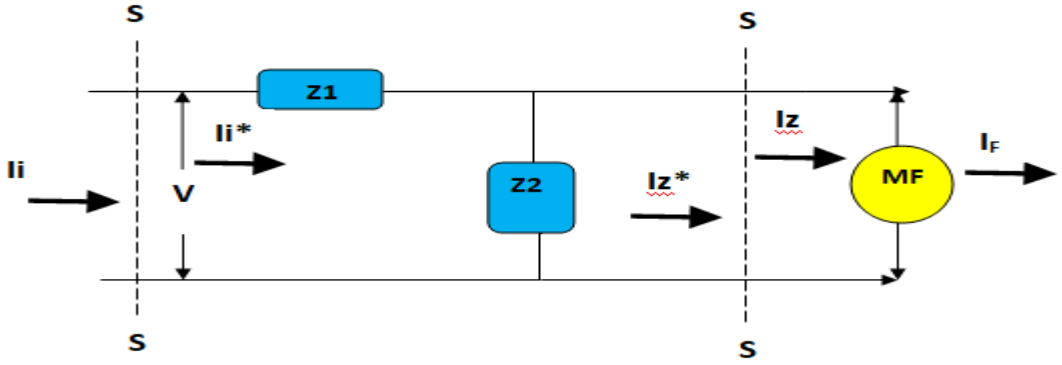

Figure 5: Simplified Intensity and Electronic Impedance Circuit

***Where — S---S; is the transducer sensor circuit converting radiation to electric current at the input and then converting from electric energy to photon energy at the output. I_i and I_i * are the incident radiation intensity and input equivalent intensity current respectively. I_z* and I_z are the output equivalent intensity current and the output radiation intensity form the impedance circuit (Z1 and Z2). MF is the metal filter and I_F is the intensity of radiation from the filter to the body tissue.*

For the parallel connection of the circuit as shown in Figure 5:

From Circuit Theorems; The total impedance for the circuit (Zt) is defined as:

$$Zt = \frac{Z1*Z2}{Z2+Z2} \qquad (1)$$

Where: Zt is the total impedance of the circuit. Z_1 and Z_2 are the input and output impedances respectively of the circuit.

Also, the individual impedances can be calculated as:

$$Z_1 = \frac{Z2*Zt}{Z2+Z2} \quad ; \quad Z_2 = \frac{Z1*Zt}{Z2+Z2} \qquad (2)$$

Assuming, the branch impedances are equal and with no reactive component($X_1 = X_2 = 0$):
Then: $Z_1 = Z_2 = R_1 = R_2$ (3)

Where: R is resistance of coil.

Therefore;

$$Zt = \frac{Z1}{2} = \frac{Z2}{2}$$

Where: From the circuit in Figure 5; Z_2 = output impedance of the circuit. (4)

Also, by definition:

$$\textit{Intensity of Radiation (I)} = Radiation\ Power(Pr) \Big/ C.S.A\ of\ medium(A) \qquad (5)$$

Where: C.S.A is Cross Sectional Area in (m^2) ; Pr in (Watt) and I in (Watt/sr)

From the principle of conservation of energy and adapting the principle of photo-electricity;

Therefore,

$$P_r = P_A \qquad (6)$$

Where: P_A is equivalent electric power from transducer sensor of X-ray radiation power

Given from Ohm's law:

$$Pt = Pa = \frac{V^2}{Zt} \quad (7)$$

Where: Pt is the total equivalent power into the circuit from the X-ray radiation

Similarly, Power output from the circuit to the metal filter is defined as:

$$P_2 = \frac{V^2}{Z2} \quad (8)$$

Where: V is the voltage of the circuit or tube voltage of the X-ray tube.

Therefore, from Equation 5, it is deduced as follows:

$$I_i = \frac{V^2}{Zt * A} \quad \text{and} \quad I_Z = \frac{V^2}{Z2 * A} \quad (9)$$

Where: I_i and I_z are the total circuit /incident and output intensity measures of and from the circuit respectively. A is the cross sectional area of the resistive coils (assuming equal dimension of the coils).

Also, as defined:

$$\textit{Energy of Radiation per volume (E)} = Intensity\ of\ Radiation(I)/Velocity\ of\ light(c) \quad (10)$$

Where: E is in unit (eV) (assuming unit volume); I in (Watt/sr) and c is (3 x10^8 m/s^2)

Therefore, merging Equations 5, 9 and 10;

$$E_i = \frac{Ii}{c} \quad \text{and} \quad E_z = \frac{Iz}{c} \quad \text{and} \quad E_F = \frac{IF}{c} \quad (11)$$

Where: E_i and E_z are the total circuit /incident and output photon Energy measures of and from the circuit respectively. E_F is the photon Energy of Intensity I_F at the metal filter.

Also, for the metal filter (F):

Using the mass absorption law;

$$I_F = I_i * e^{-\mu X} \quad (12)$$

Where: μ is the energy absorption coefficient of the metal filter of breast material, X is the thickness of the attenuating beam crossed metal filter or breast (cm or mm).

Additionally, by definition;

HVL = X ; when I_i is reduced by half.

Also,

$$\mu = M * \rho \qquad (13)$$

Where: M is the Mass energy absorption coefficient of the metal filter of breast material (cm^2/g) and ρ is the density of the metal filter, absorption material or breast (g/cm^3)

Therefore, maximum possible photon energy(Eimax) available for a X-ray Mammography;

$$E_{imax} \leq (E_z + E_F) \pm \alpha_K \qquad (14)$$

Where: α_K is the variable K-edge cut off energy level of the metal filter (eV); and E_z and E_F can be varied according to safe energy level needs.

Furthermore,

For a chain of N impedance branches (B) in a circuit;

Also assuming, the branch impedances for each parallel impedance branch are equal and with no reactive components ($X_1 = X_2 = \ldots. X_N = 0$):

Therefore, from Equation4, for a series connection of the branches (B), we then have:

$$Zt_{NB} = \frac{Z1}{2} = \frac{Z2}{2} + \frac{Z3}{2} = \frac{Z4}{2} + \ldots.. + \frac{ZN-1}{2} = \frac{ZN}{2} \qquad (15)$$

Where: Zt_{NB} = Is the total input impedance of the branched circuit and Z_N = is the output impedance of the circuit to the metal filter.

Similarly, following from Equation 9;

$$I_{iNB} = \frac{V^2}{Zt\mathrm{N} * A} \quad \text{and} \quad I_{ZN} = \frac{V^2}{ZN * A} \qquad (16)$$

Where: I_{iNB} and I_{ZN} are the total circuit /incident and output intensity measures of and from the cascaded branched circuits respectively. A is the cross sectional area of the resistive coils (assuming equal dimension of the coils).

3.4 Convolutional Neural Network (CNN) for Image Classification

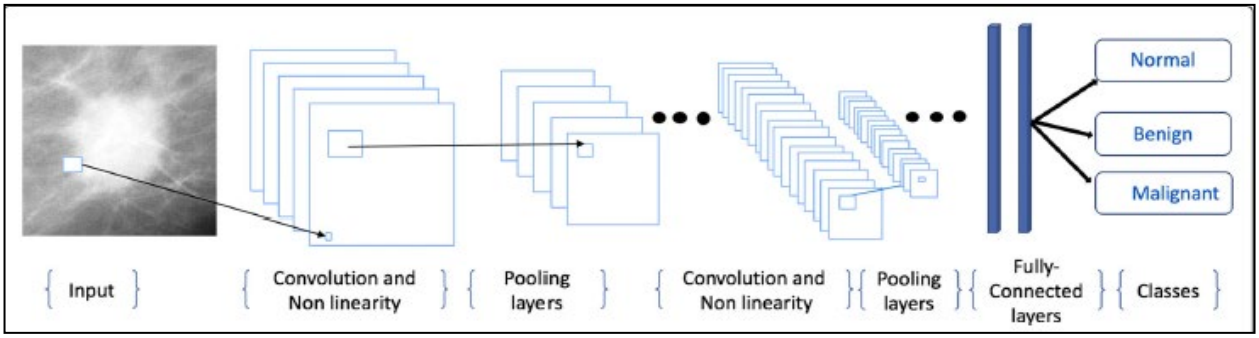

Figure 6: Typical CNN Architecture for Mammography (Abdelhafiz et al., 2017).

CNNs are actually artificial Neural Networks (ANN) optimized for image-related pattern recognition. CNNs are based on convolutional layers instead of fully connected layers. As shown in Figure 6, a convolutional layer is used to detect patterns in an image with a filter. A filter is just a matrix that is applied to a portion of an input image through a convolutional operation and the output will be another image (also called a feature map) with the highlighted patterns found by the filter (So et al., 2020).

A convolution is a specific type of matrix operation. For an input image, a filter of size **n*n** will go through a specific area of an image and apply an element-wise product and a sum and return the calculated value:

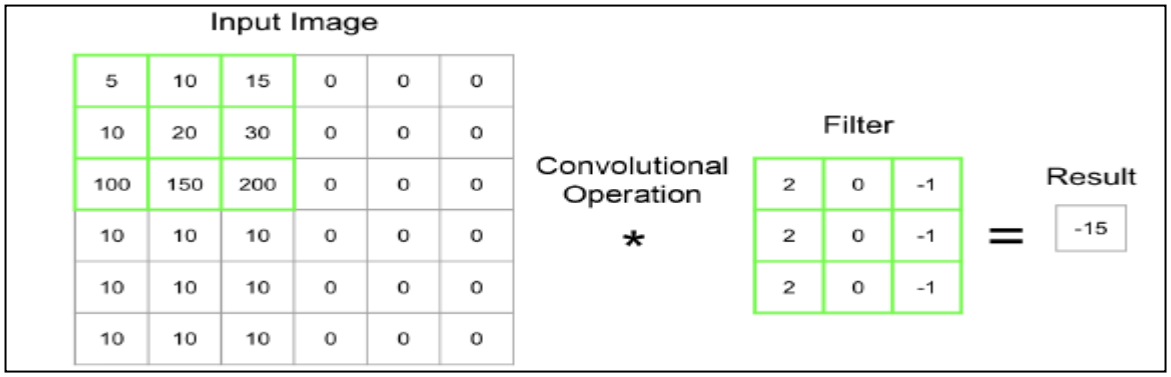

Figure 7: Convolutional operations (So et al., 2020)

In Figure 7, we applied a filter to the top-left part of the image. We then apply element-wise multiplication; then we will perform the same operation by sliding the filter to the right by one column from the input image. We keep sliding the filter until we have covered the entire image. Rather than sliding column by column, we can also slide by two, three, or more columns. The parameter defining the length of this sliding operation is called the **stride** (So et al., 2020) . Furthermore, since a convolutional operation tend to decrease the size of an image after processing, we can retain the dimension of the image by applying **padding**; which is the addition of rows and columns with the value 0 around the border of the input image. A convolutional layer is just the application of the convolutional operation with multiple filters.

3.4.1 Analytical Estimation of Pooling for CNN

A pooling layer is a matrix of a given size and will apply an aggregation function to each area of the feature map. The most frequent aggregation method is finding the maximum value of a group of pixels:

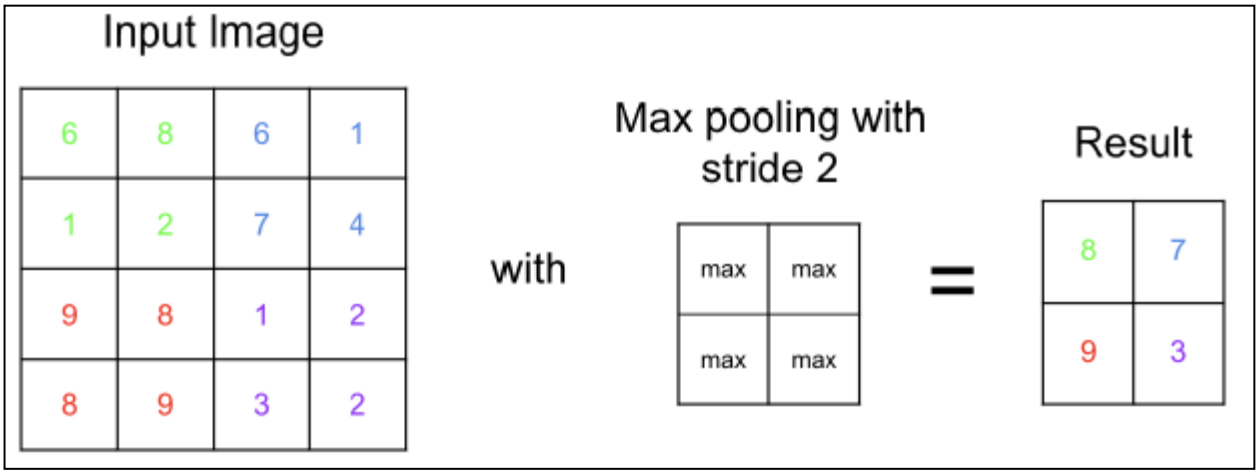

Figure 8: Example working of the pooling area (So et al., 2020)

From the background theories of the CNN as briefly described; it can be deduced that, the number of pooling layers are proportional to the validation accuracy score of the CNN model; with the required number of classes a factor in such proportional relationship, for the classification simulation.

From the mathematical description of direct proportionality;

$$P^{\frac{1}{c+1}} \propto a \quad (17)$$

Therefore,

$$P^{\frac{1}{c+1}} = \gamma * a \quad (18)$$

Where: c is the number of images classes to be resolved; γ is the constant factor, is a function of other non-changing parameters in the model, for example pooling size, stride, filter size and the specific CNN architecture employed. P is the estimated number of pooling layers required and a is the target or expected validation accuracy of the CNN model for the specific number of pooling layers or convolution-pooling layers (i.e. since the number of convolution layers is usually taken as the same amount as the number of pooling layers).

Now, resolving the proportional relationship;

$$\frac{\sqrt[c+1]{P1}}{a1} = \frac{\sqrt[c+1]{P2}}{a2} \quad (19)$$

Where: P1 and a1 are the initial number or reference number of pooling layer(s) and the initial or reference validation score respectively. Also, P2 and a2 are the target number of pooling layer(s) and the final or target validation score respectively.
Finally, by also incorporating padding; the estimated number of pooling layers (N_P) is thus:

$$N_P \approx P2 + 1 \quad (20)$$

Since the number of Convolutional layers is usually used as the same as the pooling layers, therefore, the number of estimated Conv-pool layers is also N_P .

4. RESULTS AND DISCUSSION

This section outlines the results obtained and the various associated interpretations, and discussions on the results obtained in harmony with theories derived and literature obtained.

4.1 Dense Breast X ray exposure analysis

Table 1: Radiation Exposure Settings for 2D FFDM, 3D Tomosynthesis, and CESM Studies of Dense and Non-Dense Breast Tissues

Filter Type---Imaging Technique	Filter K-Edge Energy Cut off (keV)	Photon Energy (keV)	Breast Thickness (cm)	Tube Current–Time Product (per 10 mAs) (** Dense Breast)	Tube Current–Time Product (per 10 mAs) (** Non-Dense Breast)
Rh ---2D FFDM	23.3	25	1.1	2.7	2.5
Rh ---2D FFDM	23.3	28	2	3.1	4.4
Rh ---2D FFDM	23.3	26	3	7.6	6.4
Rh ---2D FFDM	23.3	28	4	9.7	7.7
Rh ---2D FFDM	23.3	29	5	15.2	11.8
Rh ---2D FFDM	23.3	31	6	24	17.6
Al ---3D tomosynthesis	1.56	26	1.1	3	3
Al ---3D tomosynthesis	1.56	26	2.1	3.8	3.3
Al ---3D tomosynthesis	1.56	28	3.1	3.8	3.4
Al ---3D tomosynthesis	1.56	29	4.1	5	4.4
Al ---3D tomosynthesis	1.56	31	5.1	5.7	5
Al ---3D tomosynthesis	1.56	33	6.1	6.9	6.4
Rh ---CESM (Low Energy)	23.3	26	1.1	2.4	2.3
Rh ---CESM (Low Energy)	23.3	26	2	4.4	3.9
Rh ---CESM (Low Energy)	23.3	26	3	8.2	6.8
Rh ---CESM (Low Energy)	23.3	28	4	10.4	8.3
Ag ---CESM (Low Energy)	25.51	29	5	12.1	9.7
Ag ---CESM (Low Energy)	25.51	31	6	19	14.2
Cu ---CESM (High Energy)	8.98	45	1.1	3.2	2.9
Cu ---CESM (High Energy)	8.98	45	2	5.7	4.6
Cu ---CESM (High Energy)	8.98	45	3	8.4	5.7
Cu ---CESM (High Energy)	8.98	45	4	11.4	9
Cu ---CESM (High Energy)	8.98	49	5	10.5	8.2
Cu ---CESM (High Energy)	8.98	49	6	18.7	13.8

(Data Source: (James, 2017)

***Note— Each slab contained two tissue-equivalent materials mimicking 100% fatty and 100% glandular tissues in ratios of approximately 50:50 (nondense) and 70:30 (dense) by weight. FFDM = full-field digital mammography, CESM = contrast-enhanced spectral mammography, Rh = rhodium, Al = aluminum, Ag = silver, Cu = copper.*

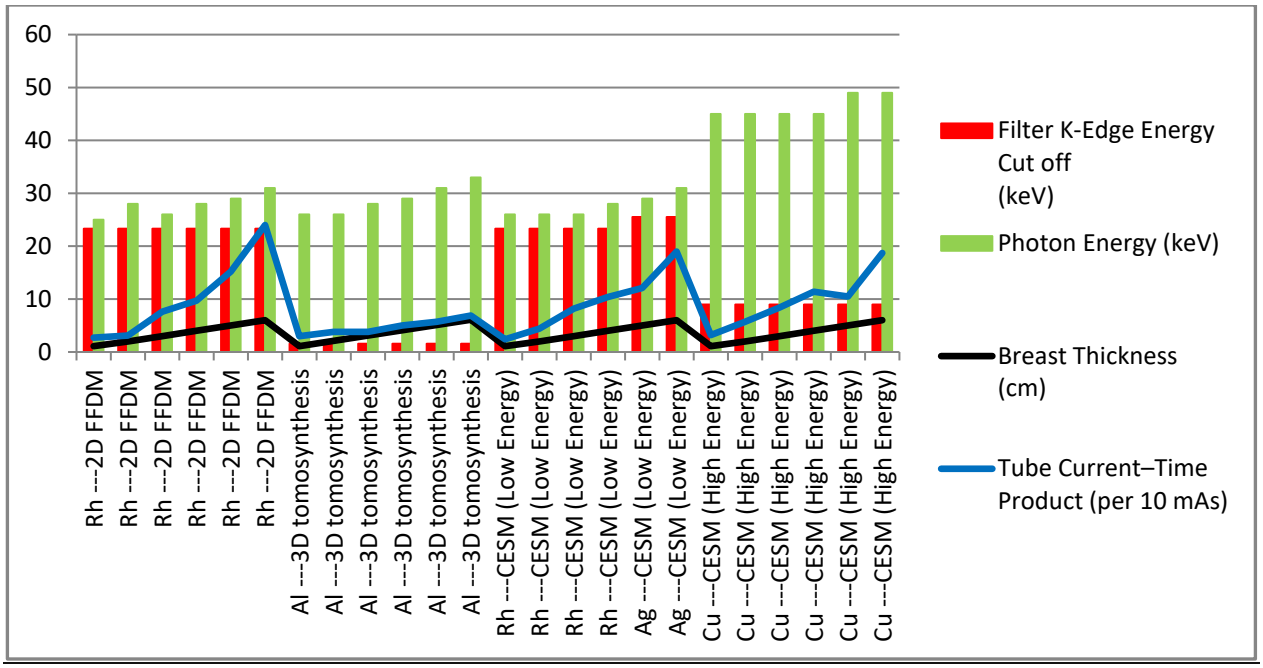

Figure 9: Plot of Dense breast, Imaging Technique and Energy relationships

As shown in the profile plot in Figure 9 for a Dense breast, using Table 1; the imaging techniques (2D FFDM, 3D tomosynthesis, CESM), have photon energies that increases with breast thickness, in an estimated even ratio of (2-3%) as shown. Additionally, the tube current which is also a function of the imaging technique/Xray equipment also increases with breast thickness, with the most minimal increase noticed with the 3D tomosynthesis technique.

Furthermore, filter types K-edge Energy value is lesser than and also not proportional to the photon energy of the xray imaging equipment. For specific (Metal) filter types, it is shown that Rh and Ag both have more than a 50% greater comparative value of K-Edge than Cu and Al (which has the least K-edge value). Also, the plots indicates that the CESM (High Energy Imaging type) has a greater photon energy (more than a 40% greater comparative value) than other imaging techniques analysed; but the CESM(Low Energy Imaging type) is nearly equivalent (with a 1-2% variations) to the 2DFFDM and 3D tomosynthesis imaging techniques. From the plots in Figure 9 and analysed results for a Dense breast, the imaging techniques (2D FFDM, 3D tomosynthesis, CESM); the photon energy expectedly increases as breast thickness increases; such energy increases is noticeably not related to the K-edge cut off energy, which is the inherent characteristics of the metal filter; thereby indicating that for quality xrays, as photon energy from the xray equipment increases, such can be balanced by selecting the

appropriate metal filter with the K-edge cut-off energy, large enough to provide a safer level of radiation reaching the human tissue; this makes metal filters of higher K-edge cutoff more suitable for xray activities. It is already noted that low energy xrays are usually absorbed by the body tissue and thereby increase the absorbed dosage, so energy levels above 15KeV, are usually recommended for breast cancer xrays (Mowlavi, 2005). Also, though Rh indicates the highest energy potential from the comparative analysis; to effectively optimize and manage resources; a combination of metals can be used to achieve a target K-edge cut off and even produce a much more energy efficient and effective system as required for not only a quality an xray procedure, but a safer one with better protection from harmful radiations. Some recent studies have also shown that different metal target filter combinations, such as : Mo-Rh, W-Rh, Rh-Al, reported about 50% decrease of the average glandular dosage, when compared with a metal filter of one type or one type combination like Mo-Mo (Dance, Thilander, Sandborg, Skinner, Castellano, Alm, 2000; Thilander, Ackerholm, Berlin, Bjurstam, Mattsson et al., 1997; Jennings, Eastgate, Siedband, Ergun, 1981). Additionally, for a dense breast, the tube current from the xray equipment, increases more sharply and greatly as breast thickness increases, indicating the need for more x-ray tube current for a period of exposure to create better quality imaging as breast thickness increases. Interestingly, from the analysis combining the metal filters qualities and the imaging technique, it is observed that the tube current within a given time of exposure, is most affected by the filter characteristics and the thickness of the breast; as it shows minimal values even for section with high x-ray energy, further suggesting that, the tube current can be optimized, varied and also practically controlled by appropriately adjusting it to suit the breast thickness and in harmony with the unique metal filter deployed, to ensure a safer procedure, especially when using x-rays of too high energy or too low (irradiation) energy. For the techniques analysed, the CESM indicates the most efficiency as an imaging technique for low and high energy; but also other techniques analysed show some efficiency and can be utilized for specific purposes(when also combined with the adequate metal filter), for example for mammography that requires low energy x-rays. As also confirmed by some experiments, CESM has shown higher diagnostic accuracy than 2D FFDM and could even be compared with the accuracy of breast MRI (Hobbs, Taylor, Buzynski, Peake, 2015; Fallenberg, Dromain, Diekmann et al., 2014; Thibault, Balleyguier, Tardivon, Dromain, 2012; Jochelson, Dershaw, Sung et al., 2013). Furthermore, though CESM has the tendency to add further radiation

dosage(due to its higher energy of operation) than FFDM, it shows better promise in being able to help improve radiologists' ability to differentiate between malignant and benign breast cancers for denser breasts (Dromain, Canale, Saab-Puong, Carton, Muller, Fallenberg, 2014; Fallenberg, Dromain, Diekmann, et al., 2014; Jeukens, Lalji, Meijer et al., 2014).

4.2 Non-Dense Breast X ray exposure analysis

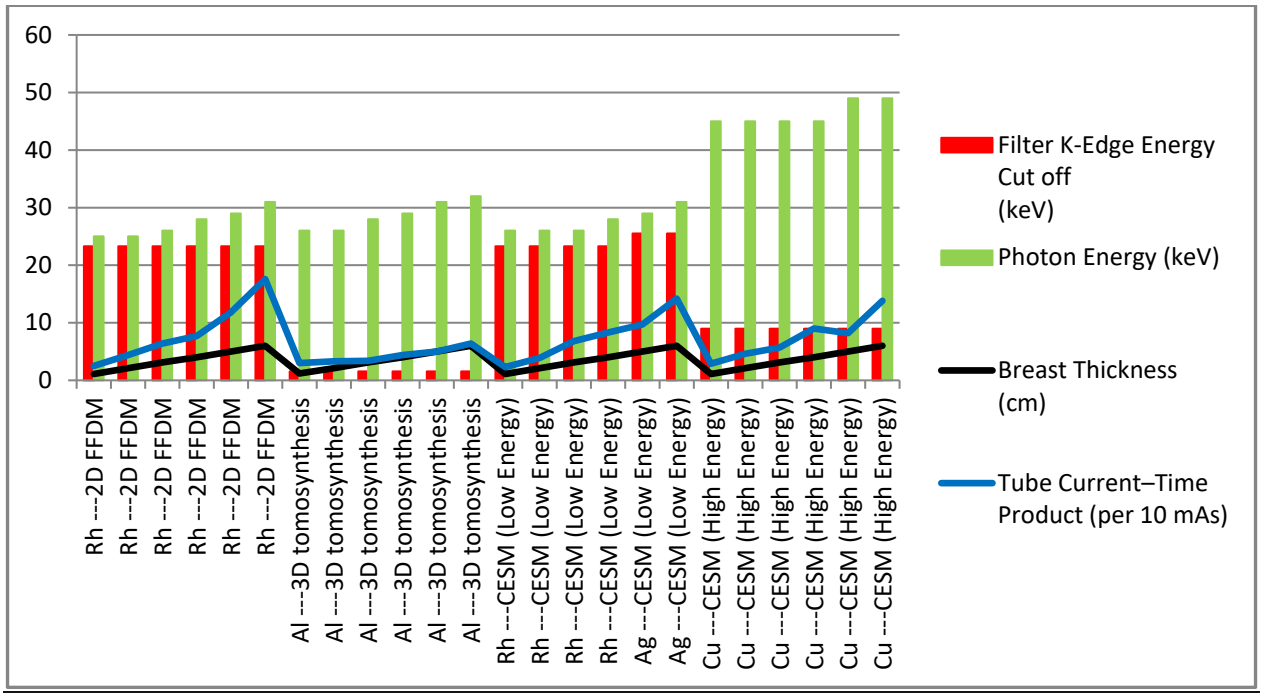

Figure 10: Plot of Non-Dense breast, Imaging Technique and Energy relationships

As shown in the profile plot in Figure 10 for a Non-Dense breast, using Table 1; the relationships and values of imaging techniques (2D FFDM, 3D tomosynthesis, CESM), photon energies and breast thickness are same as for the Dense breast. Additionally, the tube current is lower than that for the Dense breast, but also similarly increases with breast thickness, with the most minimal increase noticed with the 3D tomosynthesis technique. Furthermore, also for the Non-Dense breast, filter types K-edge Energy values are similarly lesser than and also not proportional to the photon energy of the X-ray imaging equipment; as with the Dense breast. For specific (Metal) filter types, the Non Dense breast displays similar characteristics, relationships and values as that for the Dense breast, for the analysis carried out.

From the plots in Figure 10 and analysed results for a Non-Dense breast, the imaging techniques (2D FFDM, 3D tomosynthesis, CESM); the photon energy shows similar qualities with the thickness of breast, metal filter characteristics and the K-edge and energy potentials and radiation protection abilities of the filter metals; by acting ac energy windows, filters provide an energy allowance and barrier to sustain the balance between the quality and safety of x-ray procedures (Jaffe and Maidment, 2014). Additionally, for a Non-dense breast, the tube current from the x-ray equipment, increases less sharply and lesser than that for a Dense breast, as breast thickness increases, indicating the need for a lesser x-ray tube current for a period of exposure to create better quality imaging as breast thickness increases for a Non-Dense breast. Also, noticeably, as in the case of a Dense Breast; the analysis combining the metal filters qualities and the imaging technique, shows that the tube current within a given time of exposure, is most affected by the filter characteristics and the thickness of the breast; as it shows minimal values even for sections with high x-ray energy, further suggesting that, the tube current can also be optimized for a Non-dense breast, in harmony with filter type and breast thickness, to ensure a safer procedure, especially when using x-rays of high energy. Furthermore, same as for a Dense breast, the CESM indicates the most efficiency as an imaging technique for low and high energy for a Non-Dense breast; but other techniques also showed good potential of increase in efficiency for specific purposes(when also combined with the adequate metal filter), especially for procedures that require lesser x-ray energy or varied energy systems; like the dual energy system, where the K-edge filtering technique of the filters are used to shape the low and high energy spectra and obtain an improved quasi-monochromatic spectra (Koukou et al., 2017; Koukou et al., 2017; Martini et al., 2017).

4.2 Dense Breast CESM Intensity and Circuit Impedance Analysis

Table 2: Intensity of x-ray radiation, and electronic circuit impedances for CESM Studies of Dense Breast Tissues

Filter Type---Imaging Technique	Ii (Watt/sr)	Iz (Watt/sr)	I_F (Watt/sr)	Z2 (KiloOhm)	Zt (KiloOhm)
Rh ---CESM (Low Energy)	2.086977724	1.043488862	1.049130827	0.323913376	0.647826752
Rh ---CESM (Low Energy)	2.086977724	1.043488862	1.049130827	0.323913376	0.647826752
Rh ---CESM (Low Energy)	2.086977724	1.043488862	1.049130827	0.323913376	0.647826752
Rh ---CESM (Low Energy)	2.247514472	1.123757236	1.123757236	0.348829789	0.697659579
Ag ---CESM (Low Energy)	2.327782846	1.163891423	1.167345264	0.361287996	0.722575992
Ag ---CESM (Low Energy)	2.488319594	1.244159797	1.247851834	0.38620441	0.772408819
Cu ---CESM (High Energy)	3.61207683	1.806038415	1.806640852	0.560619304	1.121238609
Cu ---CESM (High Energy)	3.61207683	1.806038415	1.806640852	0.560619304	1.121238609
Cu ---CESM (High Energy)	3.61207683	1.806038415	1.806640852	0.560619304	1.121238609
Cu ---CESM (High Energy)	3.61207683	1.806038415	1.806640852	0.560619304	1.121238609
Cu ---CESM (High Energy)	3.933150326	1.966575163	1.96723115	0.610452132	1.220904263
Cu ---CESM (High Energy)	3.933150326	1.966575163	1.96723115	0.610452132	1.220904263

Where – *Ii = incidence intensity, Iz = Intensity from electronic circuit, I_F = intensity from metal filter; Z2 = output impedance of circuit, Zt = Total impedance of circuit. Using unit Cross sectional Area of impedance coil.*

***Note— Each slab contained two tissue-equivalent materials mimicking 100% fatty and 100% glandular tissues in ratios of approximately 50:50 (nondense) and 70:30 (dense) by weight. CESM = contrast-enhanced spectral mammography, Rh = rhodium, Ag = silver, Cu = copper.* **(Data Source: (James, 2017)**

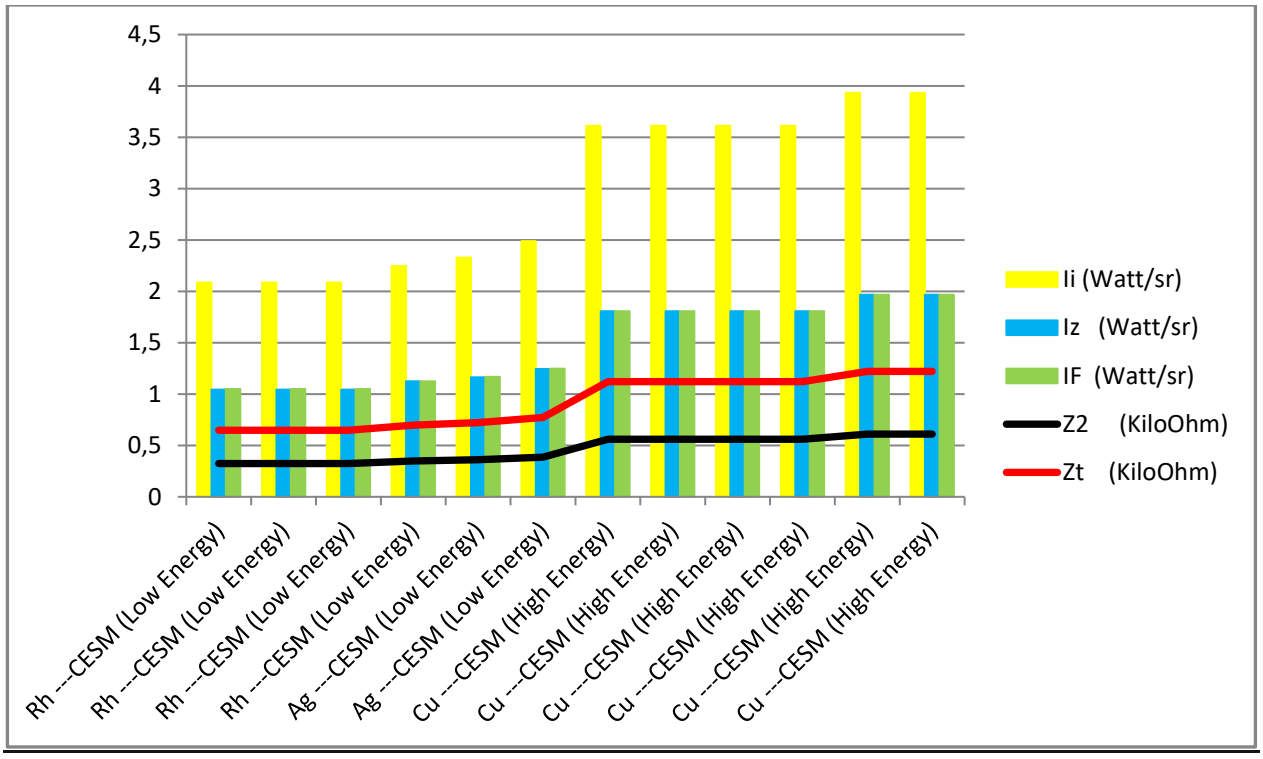

Figure 11: Plot of Dense breast, CESM Technique, Intensity and Circuit Impedance relationships

As shown in the profile plots of Figure 11 using Table 2; for a Dense breast, using the CESM imaging technique; the total intensity of the X-ray radiation is reduced by 50% by the electronic energy sensor filtering circuit; and the intensity produced by the electronic circuit is approximately equal to the intensity of the radiation by either of the Metallic Filters (Rh, or Ag, or Cu). Furthermore, the impedances of the electronic energy sensor filtering circuit, increases very minimally, between 1-2% (with the total circuit impedance being double of the output impedance value) or rather approximately constant, with corresponding increase of the total intensity of the radiation and intensity of the electronic and Metals filters, respectively; such minimally gradual increase is shown to be approximately negligible in some cases. Additionally, the impedances increases by over 90% from a low energy radiation to a high energy radiation, for the same metal filters and imaging technique.

From the plots in Figure 11 using Table 1; and analysed results for the CESM Imaging technique; the reduction in the total incident intensity by the electronic filter circuit from for low and high energy x-rays, indicates a potential for safer x-ray operation can be achieved, with also more room to increase the intensity if needed by the variation of the electronic circuit impedances. Generally, lower intensity beams are needed for x-rays, and such trade-off provided by the electronic circuit, can be exploited for greater accuracy for x-rays while minimizing harmful radiation intensity; because due to the risk of harmful radiation exposure, the possible fear of such exposure due to mammography should also be addressed (Heywang et al., 1997); because the harmful radiation energy intensity levels are checked or reduced appropriately by the electronic circuit, by varying its impedance values (Z2 and Zt) as depicted. This ensures that there is a good trade-off between x-ray radiation energy for better diagnosis and the safety of patient/body tissues from harmful radiations, because the intensity of beam arriving at the breast tissue from the metals filter, will be at an acceptably safe level; due to the radiation being processed by the initial electronic impedance circuit and further by the inherent metal filters. As also elaborated by a credible report, a risk estimate of breast cancer radiation induction which was based on available data from the International committee on Radiation Protection(ICRP) 2007 report, the scientific literature, the Biological effects of Ionizing Radiation(BEIR VII) 2006 and a previously published risk model; was provided in response to screening x-ray mammography, and helped provide a standard approximate incidence value of

radiation-induced cancers brought about by screening mammography, as a means to relate this to the baseline incidence of breast cancer in women (De Gelder, Draisma, Heijnsdijk, et al., 2011; Wrixon, 2008). Additionally, for high energy x-rays as analysed for the CESM Imaging technique; the much greater increases in radiation intensity (Iz and I_F) for both the electronic and metal filters respectively, indicates that the system provides more radiation intensity availability and also protection for high energy radiations, by a correspondingly higher intensity values compared to lower energy x-rays; but both intensities being lesser than the incident radiation intensity. Additionally, for both high and low energy x-rays, the intensity values of the electronic circuit is approximately equal to the intensity of radiation delivered by the metal filters, thereby indicating the processing ability of the electronic circuit to act as even a substitute to the metal filter or also having the potential of combination with the metal filters, to create a 'hybrid' system, that provides adequate radiation intensity levels and protection against harmful radiation levels, that can also be varied using the impedance values of the electronic circuit needed for a more accurate and safer x-ray analysis. Also, the overall approximately constant values of the electronic circuit impedances at the low energy (lower impedances) or high energy (higher impedances) levels, further indicates the electronic circuit integrity across different system conditions as required by the analysis.

4.3 Dense Breast CESM Energy and Circuit Impedance Analysis

Table 3: Energy of x-ray radiation, and electronic circuit impedances for CESM Studies of Dense Breast Tissues

Filter Type---Imaging Technique	Photon Energy (keV)	Ez (keV)	E_F (keV)	Ek (keV)	Z2 (per 100 Ohm)	Zt (per 100 Ohm)
Rh ---CESM (Low Energy)	26	13	13.07028877	23.3	3.239133759	6.478267518
Rh ---CESM (Low Energy)	26	13	13.07028877	23.3	3.239133759	6.478267518
Rh ---CESM (Low Energy)	26	13	13.07028877	23.3	3.239133759	6.478267518
Rh ---CESM (Low Energy)	28	14	14	23.3	3.488297894	6.976595789
Ag ---CESM (Low Energy)	29	14.5	14.54302867	25.51	3.612879962	7.225759924
Ag ---CESM (Low Energy)	31	15.5	15.54599616	25.51	3.862044097	7.724088195
Cu ---CESM (High Energy)	45	22.5	22.50750529	8.98	5.606193044	11.21238609
Cu ---CESM (High Energy)	45	22.5	22.50750529	8.98	5.606193044	11.21238609
Cu ---CESM (High Energy)	45	22.5	22.50750529	8.98	5.606193044	11.21238609
Cu ---CESM (High Energy)	45	22.5	22.50750529	8.98	5.606193044	11.21238609
Cu ---CESM (High Energy)	49	24.5	24.50817243	8.98	6.104521315	12.20904263

Cu ---CESM (High Energy)	49	24.5	24.50817243	8.98	6.104521315	12.20904263

Where – *Ez = Energy from electronic circuit coil, E_F = Energy from metal filter; E_K = K-Edge cut-off energy of metal filter ; Z2 = output impedance of circuit, Zt = Total impedance of circuit. Using unit Cross sectional Area of impedance coil.*

***Note— Each slab contained two tissue-equivalent materials mimicking 100% fatty and 100% glandular tissues in ratios of approximately 50:50 (nondense) and 70:30 (dense) by weight. CESM = contrast-enhanced spectral mammography, Rh = rhodium, Ag = silver, Cu = copper.* **(Data Source: (James, 2017)**

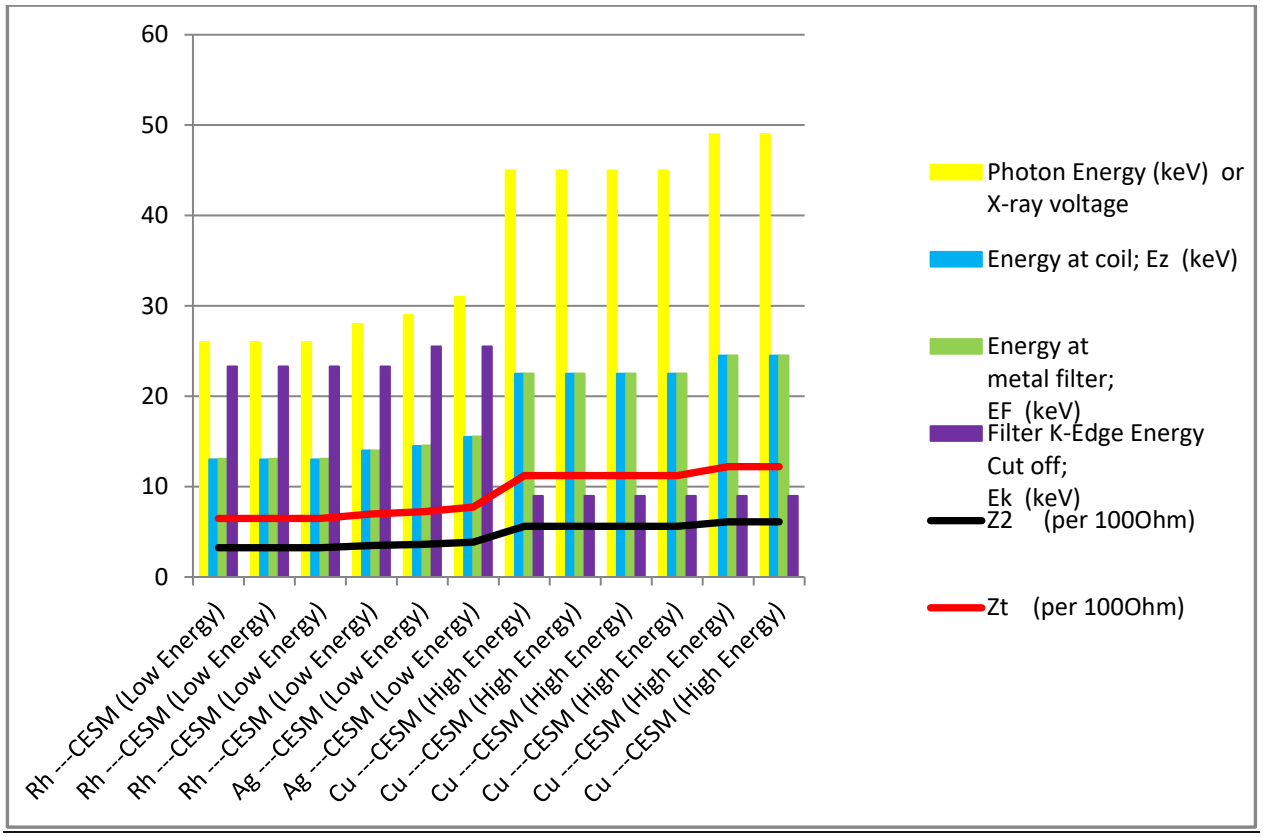

Figure 12: Plot of Dense breast, CESM Technique , Energy and Circuit Impedance relationships

As shown in the profile plots of Figure 12 using Table 3 for a Dense breast, using the CESM imaging technique; the total incident photon energy of the Xray radiation is reduced by about 50% by the electronic energy sensor filtering circuit (Ez); and the photon energy produced by the electronic circuit is approximately equal to the energy of the radiation (E_F) by either of the

Metallic Filters (Rh, or Ag, or Cu). Additionally, filter types K-edge energy values are not affected expectedly by this energy reduction achieved, which creates an interesting scenario that can be exploited.

Furthermore, the impedances of the electronic energy sensor filtering circuit, increases very minimally, between 1-2% (with the total circuit impedance being double of the output impedance value) or rather approximately constant with corresponding increase of the incident photon energy of the Xray radiation and photon energies of the electronic and Metals filters, respectively; such minimally gradual increase is shown to be approximately negligible in some cases. Additionally, the impedances increases by over 90%, from a photon/radiation energy radiation to a high energy radiation, for the same metal filters and imaging technique; while the K-edge cut off energy values remain constant for each metal filter.

From the plots in Figure 12 using Table 3 and analysed results for the CESM Imaging technique; the reduction in photon energy by the electronic circuit also in harmony with the reduction of the intensity of the radiation by the electronic filter circuit, does not affect the K-edge cut off energy of the metal filters; which indicates that the metals with a higher K-cut off energy can be utilized(which is good for better mammography); because such higher cut off K-edge filters provides a much more quasi-monochromatic beam for breast imaging, which provides better ability to separate unique tissues, this allowing for a much more improved distinction between low-contrast objects(1-2% difference), such as tissues having cancer and surrounding normal breast tissues (Hammerstein et al., 1979), while the total incident photon energy can be further increased without harmful radiations affecting the human breast. The harmful radiation energy levels are checked mated or reduced appropriately by the electronic circuit, by varying its impedance values (Z2 and Zt) as depicted. This ensures that there is a good trade-off between xray radiation energy for better diagnosis and the safety of patient/body tissues from harmful radiations, because the cumulative photon energy arriving at the breast tissue from the metals filter, will be at an acceptably safe level; as processed by the initial electronic impedance circuit and then the inherent metal filters k-edge cut off targets. Furthermore, for high energy xrays as analysed for the CESM Imaging technique; the much greater increases in photon energies (Ez and E_F) for both the electronic and metal filters respectively, indicates that the system provides more energy availability and also protection for

high energy radiations, by a correspondingly higher energies values compared to lower energy xrays; but both energy levels being lesser than the incident photon energy . Additionally, for both high and low energy xrays, the photon energy values of the electronic circuit is approximately equal to the energy of the radiation delivered by the metal filters, thereby indicating the processing ability of the electronic circuit to act as even a substitute to the metal filter or also having the potential of combination with the metal filters, to create a 'hybrid' system, that provides adequate energy levels and protection against harmful radiation levels, that can also be varied using the impedance values of the electronic circuit needed for a more accurate and safer xray analysis. Also, the overall approximately constant values of the electronic circuit impedances at the low energy (lower impedances) or high energy (higher impedances) levels, further indicates the electronic circuit integrity across different system conditions as required by the analysis.

4.4 Dense Breast CESM HVL and Circuit Impedance Analysis

Table 4: HVL of x-ray radiation mammography, and electronic circuit impedances for CESM Studies of Dense Breast Tissues

Where – *HVL= Half value layer in mammography; Z2 = output impedance of circuit, Zt = Total impedance of circuit.*

Filter Type---Imaging Technique	HVL (for circuit) (mm)	HVL measured at filter (mm)	Breast Thickness(cm)	Z2 (KiloOhm)	Zt (KiloOhm)
Rh ---CESM (Low Energy)	0.21682606	0.497	1.1	0.323913376	0.647826752
Rh ---CESM (Low Energy)	0.21682606	0.497	2.1	0.323913376	0.647826752
Rh ---CESM (Low Energy)	0.21682606	0.497	3.1	0.323913376	0.647826752
Rh ---CESM (Low Energy)	0.329010984	0.529	4	0.348829789	0.697659579
Ag ---CESM (Low Energy)	0.395974802	0.575	5	0.361287996	0.722575992
Ag ---CESM (Low Energy)	0.395974802	0.608	6	0.38620441	0.772408819
Cu ---CESM (High Energy)	3.531448374	3.13	1.1	0.560619304	1.121238609
Cu ---CESM (High Energy)	3.531448374	3.13	2.1	0.560619304	1.121238609
Cu ---CESM (High Energy)	3.531448374	3.13	3.1	0.560619304	1.121238609
Cu ---CESM (High Energy)	3.531448374	3.13	4	0.560619304	1.121238609
Cu ---CESM (High Energy)	3.531448374	3.386	5	0.610452132	1.220904263
Cu ---CESM (High Energy)	3.531448374	3.386	6	0.610452132	1.220904263

***Note— Each slab contained two tissue-equivalent materials mimicking 100% fatty and 100% glandular tissues in ratios of approximately 50:50 (nondense) and 70:30 (dense) by weight. CESM = contrast-enhanced spectral mammography, Rh = rhodium, Ag = silver, Cu = copper.* **(Data Source: (James, 2017)**

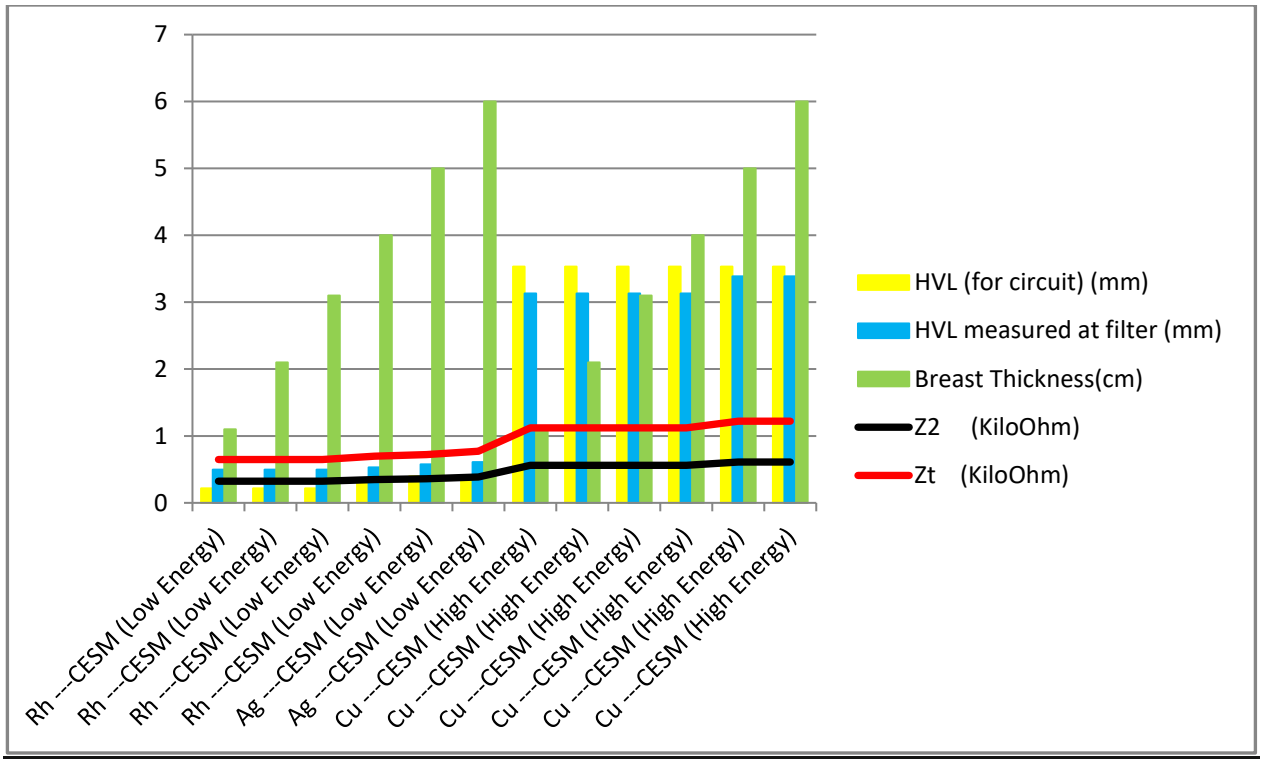

Figure 13: Plot of Dense breast, CESM Technique , HVL and Circuit Impedance relationships

As shown in the profile plots of Figure 13 using Table 4 for a Dense breast, using the CESM imaging technique; for a lower energy x-ray, the HVL of both the electronic circuit and metal filters, increase by about 3-5%, as breast thickness increases by over 90%. Also, for lower energy x-rays, the HVL of the electronic circuit is about 50% lesser than that provided by the respective metal filters analysed. Additionally and alternatively, for high energy x-rays, the plots indicate that the HVL of the electronic circuit is greater than that of the metallic filters, by about 5-10%, which is significant and further creates a design interest. Furthermore, the impedances of the electronic energy sensor filtering circuit, increases very minimally, between 1-2% (with the total circuit impedance being double of the output impedance value) or rather approximately constant, with corresponding minimal increases in the HVL values of the electronic and Metals filters, respectively. Additionally, the impedances increases by over 90% from a photon/radiation energy radiation to a high energy radiation, for the same metal filters, and imaging technique. Also, for a higher energy x-ray radiation, while the HVL value of the electronic circuit remains approximately constant, that of the filter increases slightly for each metal filter; as breast thickness increases.

From the plots in Figure 13 using Table 4 and analysed results for the CESM Imaging technique; the observed slight increases in HVL for both the electronic circuit and the metal filters as breast increase for lower energy x-rays, indicates that as energy of radiation expectedly increases for a thicker breast, the systems still provides some amount of protection against harmful radiation, by the corresponding increase in HVL values; additionally, this slight increase in HVL, though small, is quite significant, as typical low energy x-ray, poses lesser harm from radiation; because accompanying recent numerical increases in yearly performed mammograms, is a growing concern for long-term effects of radiation; thereby indicating the importance of HVL and measuring the amount of radiation to the breast (Culliton, 1976; Final reports of National Cancer Institute Ad Hoc, 1977; Lester, 1977). However, this slight increase in HVL for lower energy x-rays, will become inadequate when there is a large increase in breast thickness. Also, at lower energy levels, the HVL of the electronic circuit is not as large as that of the metal filter, thereby indicating that because there is lesser radiation harm from the low energy x-ray, the electronic circuit responds with a lesser HVL value and lesser impedance values (Z2 and Zt); thereby intelligently balancing the needed x-ray energy for effective and safe use and the amount that can be safely passed to the body/breast tissue; but in this case the metal filter responds with greater sensitivity due to its inert metal nature, and provides a higher HVL for low energy x-ray.

Furthermore, for a high energy x-rays as analysed for the CESM Imaging technique; the much greater increases in HVL for both the electronic and metal filters, expectedly indicates that the system provides more protection against high energy radiations, by a correspondingly higher HVL values compared to lower energy x-rays. Additionally, typical thicker breasts examinations will require higher energy x-rays, and thereby the HVL values increases as thickness of breast increases, thereby providing significant protection for the body tissues, against even very large thickness of breast, because the HVL is the thickness of the specified material that attenuates the beam of radiation to the extent that the AKR is reduced to half its original value, thereby improving unwanted radiation protection even as breast thickness increases (IAEA, 2010). Also, for high energy x-rays, the HVL values of the electronic circuit higher than that from the metal filters, as the impedances of the electronic circuit (Z2 and Zt)

increase in response to the higher radiation energy; thereby increasing the potential of the electronic circuits to provide even better protection from harmful radiations that are typical with high energy radiations, inline with the half reduction of beam intensity that HVL values indicate. This further provides the potential of the x-ray system to have more room to increase, decrease or vary energy for better flexible analysis; while the electronic circuit and with also the possible combination of the metal filters, can create a 'hybrid' system, that provides increased protection even with higher energy levels needed for a more accurate x-ray analysis (with a lesser 'total/combined' x-ray radiation energy). This system then provides a better trade-off between x-ray radiation energy for better diagnosis and the safety of patient/body tissues from harmful radiations. The overall approximately constant values of the electronic circuit impedances at the low Energy or high energy levels, further indicates the electronic circuit integrity across different system conditions as required by the analysis.

4.6 Breast Cancer Mammography Image Classification using CNN and Data Analysis

As earlier described in the methodology, the convolutional neural network (CNN) deep learning and artificial intelligent algorithm for image classification was employed to analyse and classify a few datasets (a total of 20 breast cancer mammographic images, where 10 were for **benign** and 10 for **malignant** classes, respectively). The maximum pixel size of the pooling layer is also (2,2) and the pooling stride is also 2. By using the ReLU activation function, which is the most used activation function in the world right now; results were first obtained with one convolution and one pooling layer system, and the results shown in Figure 14. **For Benign Tumor Datasets:** Data Source - https://ieee-dataport.org/open-access/benign-breast-tumor-dataset (IEEE DataPort) ; and **For Malignant Breast Cancer Images**: Data Source - https://www.kaggle.com/datasets/ramanathansp20/inbreast-dataset (INbreast Data base)

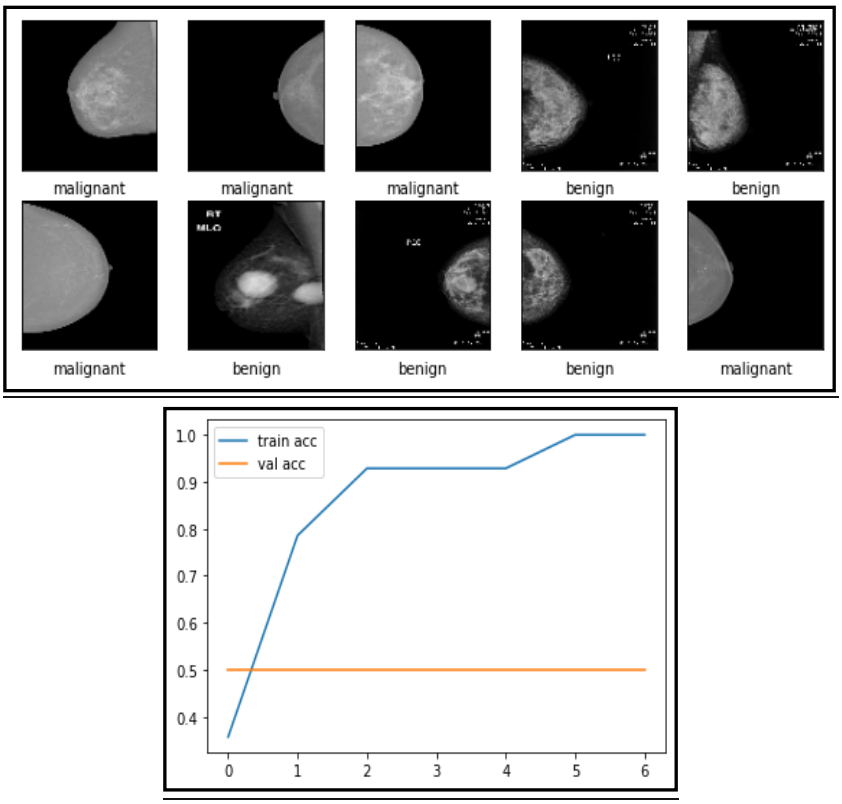

Figure 14 : Benign and Malignant breast cancer classifications and accuracy profile (1 Pooling layer)

Table 5 : Reference validation accuracy measurement for 1 pooling(reference) layer

Reference Validation Accuracy *(** as measured **(a1))***	**Number of Pooling layer** *(** as reference **(P1))***	**Max. Pooling size**
0.50	1	(2,2)

From the results obtained and analysed in Figure 14, using just one pooling layer as well as one classification layer, the classification achieved a validation accuracy of 0.50 (50%), where as the training accuracy was obtained as 1.00 (100%); implying that the exact identical images were used for both training and testing. Here also, as shown, the images in Figure 14 were classified correctly into the two classes of benign and malignant breast cancers; and for a practical situation with a hug set of data, such automated AI –driven classification, makes the process of X-ray image processing and diagnosis much more efficient. This validation accuracy is at an average level as shown in Table 5, but this value is not good enough; it therefore implies

that there are errors and the accuracy for validating non-training dataset used for the generalization ability of the model for the images, is fair. For such a case, more pooling layers are thereby needed for a better and model of higher validation accuracy and therefore even better image classification, which becomes pertinent when analysing a larger amount of x-ray images. For the accuracy of the model, using one pooling layer; the f1-scoreobtained was about 0.67(67%) which is fairly good, indicating that the model has done an above average job of predicting and classifying the images. For a real life situation as this case, the f1-score is of most importance and a better metric due to the presence of imbalance class distributions which usually associated with real life datasets.

Furthermore, now, applying Equations 17-20, as described in the methodology; we can mathematically and intelligently determine the maximum amount of pooling layers needed to obtain a target validation accuracy score. This is a helpful innovative step in the optimization process of the CNN image classification, to avoid using up more resources or layers than needed. By using the validation accuracy (**a1**) for one pooling layer as a reference point; and our target validation point or score as 75% (0.75); the maximum layer need to achieve the target validation score is calculated to be : 4.38, using Equations 19 and 20. This therefore indicates that a maximum of about 4 pooling layers and also convolution layers are needed to achieve 0.75 validation score, using the amount of image datasets and number of classes (i.e. 2) we used. When the same model was analysed, using the same conditions; 4 layers of pooling, confirmed the validation score of 0.75.

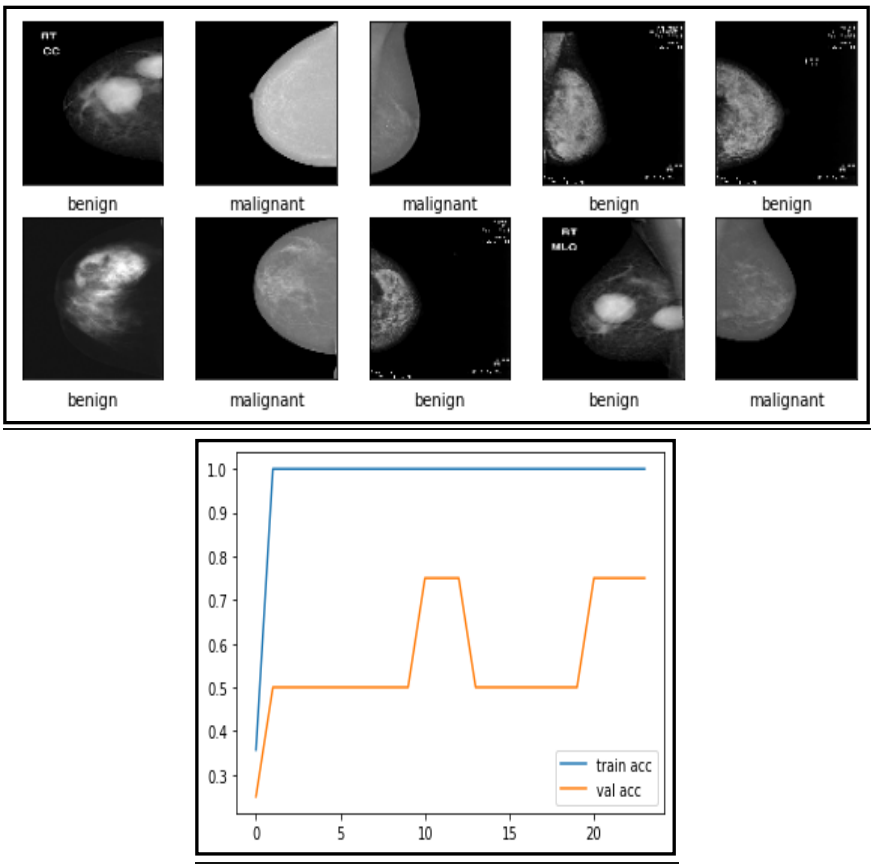

Figure 15 : Benign and Malignant breast cancer classifications and accuracy profile (4 Pooling layers)

Table 6: Target validation accuracy measurement for 4 pooling (obtained) layer

Targeted Validation Accuracy *(** as measured **(a2)**)*	**Target (N_P) layer** *(** estimated theoretically)*	**Target (N_P) layer** *(** measured)*	**Max. Pooling size**
0.75	4.38	4	(2,2)

From Figure15, the classification achieved a validation accuracy of 0.75, whereas the training accuracy was obtained as 1.00; implying that the exact identical images were used for both training and testing. Here also, as shown the images in Figure 15 were classified correctly into the two classes of benign and malignant breast cancers; and for a practical situation with a hug set of data, such automated AI –driven classification, makes the process of X-ray image processing and diagnosis much more efficient. This validation accuracy is at a good level as shown in Table 6, and this value is good enough; it therefore implies that there are fewer errors and the accuracy for validating non-training dataset used for the generalization ability of the model for the images, is very good. For such a case, the numbers of poling layers are adequate to achieve the targeted validation score, within the same dataset and system conditions. This indicates that for an efficient and optimized intelligent, CNN image classification system for x-ray images; the maximum number of pooling layers can be intelligently estimated and also predicted, to ensure a more efficient and effective x-ray image analysis and classification process, which is vital for excellent x-ray procedures and analyses. Also, generally, activation accuracy will increase with a greater number of datasets. For the accuracy of the model, using four pooling layer; the ***f1-score*** is about (80%) which is very good and indicates the model has done a very good and precise job of predicting and classifying the images.

Furthermore, the results suggest that, such an optimized CNN analysis system can also contribute to energy efficient x-ray procedures, by utilizing exact or less resources to achieve excellent image classification quality, needed for better breast cancer and other cancerous imaging analysis, diagnosis and treatments; which would also relate to the CNN architecture employed, where some of the most commonly used pre-trained CNN architectures for mammography are: (Alex-Net (IAEA, 2010; Huynh, L, Giger, 2016; Gallego-Posada, Montoya-Zapata, Quintero-Montoya, 2016; Levy, Jain, 2016; Suzuki, Zhang, Homma, Ichiji, Sugita, Kawasumi et al., 2016; Jiang, Liu, Yu, Xie, 2017; Samala, Chan, Hadjiiski, Helvie, Cha, 2017; Carneiro, Nascimento, Bradley, 2017; Mohamed, Berg, Peng, Luo, Jankowitz, Wu, 2017; Xi, Shu, Goubran, 2018; Zhang, Zhang, Han, Jacobs, Han, Wang et al., 2017), VGG16 (Gallego-Posada, Montoya-Zapata, Quintero-Montoya, 2016; Xi, Shu, Goubran, 2018; Shen, 2017), etc.).

5. LIMITATIONS AND RECOMMENDATIONS OF STUDY

This research study was focused on the data driven energy and resource based optimization analyses of breast cancer diagnostic x-ray techniques and image classifications, using analytics and deep learning artificial intelligence CNN algorithm; for a more efficient and safer x-ray procedure. Though a focused and insightful analyses of selected x-ray techniques, its relation to metal filters, the use of electronic engineering principles and artificial intelligence; there were also a few limitations within the scope of this study. In terms of data acquisition, the datasets used were from approved and dedicated data stores, repositories and databanks; which did not cover every aspect of human x-ray diagnosis and cancer related analyses; for example, age, other human physiological and demographic factors, were not covered. An example of this is from a breast Imaging Report and Data system from the American college of Radiology, which reports four major breast parenchymal patterns that are mainly used in mammography reports, states that "fatty" breasts have the least amount of fibro-glandular tissues and "extremely" dense breasts having the most fibro-glandular tissues. Furthermore, it states that over half of women younger than 50 years and a third of women above 50 years, have what is considered a dense breast tissue; and for the women with the densest breast, about 30-48% level of mammography sensitivity is achieved, which is quite low, but is also found to be a major risk factor for interval cancers (EA, D'Orsi, Bassett et al., 2013; Stomper, D'Souza, DiNitto, Arredondo, 1996; Mandelson, Oestreicher , Porter et al., 2000; Kolb, Lichy, Newhouse, 2002). Additionally, the analyses did not involve direct patients tests which could further add more perspectives to the study; with respect to other factors that may influence the results or image datasets. Also, for the CNN image classification analysis, a larger data set for even deeper layers of processing, and using a multi-view (MV) CNNs to embed more information for better performance; are a few ways to further expand the analyses (Abdelhafiz et al., 2017).

Furthermore, for the metal filter analyses, a list of the most commonly used filters for x-ray and mammography was analysed. However, this list was non-exhaustive, as some filters which are also in use with respect to x-ray examinations, were not included; to ensure a more focused approach of the research work with respect to real life applications. Further analysis on more filters are also welcomed and would provide even more analysis that can provide additional

insights on how such can be used for an optimal, safe and efficient breast cancer(mammography) x-ray procedure.

These unique analytical approaches, electronic circuit incorporation to the x-ray system, AI-CNN analysis, and proposed theories, can be further investigated; with potential applications to a variety of human cancer situations and other medical ailments, so as to further explore and extend the potentials of such techniques and systems. All these promises even greater insights with respect to further developments for modern Data and AI-Driven cancer and healthcare services; as more bridges are being built between clinical, cancer researchers, data, machine learning and AI experts to create major collaborative opportunities (Kahles et al., 2018)

6. CONCLUSIONS

There is no doubt that data and AI driven systems are at the heart of modern medical science, researchers and practices; and cancer being a major cause of health related ailment and deaths, would need to continually be tackled with the use of modern data driven processes and technologies for the benefit of humanity. Therefore, breast cancer and its associated harmful radiation effects which is a major cause for mortality in women, needs to be continually studied, researched, and treated optimally with innovative measures, processes, systems and technologies which not only should provide quality assessments, diagnosis, treatments; but must also resolve the harmful effect of unwanted radiations suffered by patients during breast cancer treatments; thereby creating an optimal, efficient(medical and energy) and safer breast cancer treatment, management and eradication processes.

Datasets (including breast scan images) from trustworthy and recognized data stores, articles, portals, and sources were used for this study's research work, analyses, demonstrations and investigations; as a result, it may be assumed that the datasets are reliable and credible. This analytical research work which was carried out between October 2022 to January 2022 as a series of methodological and methodical analyses of how different factors and systems affecting breast cancer diagnosis and treatments using X-ray mammography, with respect to density of breasts. The data analytics tools, theories, procedures employed to measure, analyse, investigate, deduce, study and draw meaningful conclusions, delivered insights and interesting

postulations on how such factors and systems can be optimized to be more efficient, safer and also deliver more quality x-ray mammography and image classification procedures for the benefit of cancer patients and survivors. These of course, is also in harmony with the 'green' industry initiative world-wide, which is aimed at making systems more energy efficient while improving performance, as for example, reducing the intensity of x-ray beams while maintaining required energy levels, is pertinent for a safer, effective and efficient x-ray mammography procedures.

The results obtained can serve as a background to even more work in these areas and expand research beyond the scope of this work, to create more results that can serve to further improve cancer research, diagnosis, treatments and management procedures in a cost effective and efficient manner, using modern analytical and data-driven Deep learning, Artificial Intelligent and Electronic Engineering solutions. With continuous improvements, the use of Artificial Intelligence, Machine/Deep Learning, Data Analytics and multidisciplinary tools in medical practices are a frontier in medicine; as exemplified by current works in early diagnosis and prevention, drug discovery, matching patients to clinical trials, treatment decisions and personalized medicine; and such will ensure that medical practices and professionals are better equipped to provide a more precise, effective, efficient, safer and robust healthcare for now and the future.

REFERENCES

Abdelhafiz. D. et al. (2017). Deep convolutional neural networks for mammography: advances, challenges and applications. From 7th IEEE International Conference on Computational Advances in Bio and Medical Sciences (ICCABS 2017) Orlando, FL, USA. 19-21 October 2017.

Ahn CK, Heo C, Jin H, Kim JH. (2017). A Novel Deep Learning-based Approach to High Accuracy Breast Density Estimation in Digital Mammography. In: SPIE Medical Imaging. International Society for Optics and Photonics. p. 101342O–101342O.

American College of Radiology (ACR) (2013). ACR BI-RADS® mammography. In: Sickles EA, D'Orsi CJ, Bassett LW, et al, editors. ACR BI-RADS® Atlas: Breast Imaging Reporting and Data System. 5th ed. Reston (VA): American College of Radiology.

Becker AS, Marcon M, Ghafoor S, Wurnig MC, Frauenfelder T, Boss A. (2017). Deep learning in mammography: diagnostic accuracy of a multipurpose image analysis software in the detection of breast cancer. Investig Radiol.;52(7):434–40.

Ben-Ari R, Akselrod-Ballin A, Karlinsky L, Hashoul S. (2017). Domain specific convolutional neural nets for detection of architectural distortion in mammograms. In: Biomedical Imaging (ISBI 2017) 2017 IEEE 14th International Symposium on IEEE. 2017. p. 552–6.

Boyd NF, Lockwood GA, Martin LJ, Byng JW, Yaffe MJ, Tritchler DL. (2001). Mammographic density as a marker of susceptibility to breast cancer: a hypothesis. IARC Sci. Publ.154:163-169.

Brandan, M.E.; Ramirez, V.R. (2006). Evaluation of dual-energy subtraction of digital mammography images under conditions found in a commercial unit. Phys. Med. Biol, 51, 2307–2320.

Carbonaro LA, Di Leo G, Clauser P, et al. (2016). Impact on the recall rate of digital breast tomosynthesis as an adjunct to digital mammography in the screening setting: a double reading experience and review of the literature. Eur J Radiol 2016; 85:808–814

Carneiro G, Nascimento J, Bradley AP.(2017). Automated Analysis of Unregistered Multi-View Mammograms With Deep Learning. IEEE Trans Med Imaging. 2017;11(36):2355–65.

Carneiro G, Nascimento J, Bradley AP. (2015). Unregvistered multiview mammogram analysiswith pre-trained deep learning models. In: International Conference on Medical Image Computing and Computer-Assisted Intervention. Springer. p. 652–60.

Chamieh C, et al. (2022). Statistical methods for evaluating the fine needle aspiration cytology procedure in breast cancer diagnosis. BMC Med Res Methodol;22.

Chartrand G, Cheng PM, Vorontsov E, Drozdzal M, Turcotte S, Pal CJ, et al. (2017). DeepLearning: APrimer for Radiologist RadioGraphics.;7(37):2113–31.

Cheung YC, Lin YC, Wan YL, et al. (2014). Diagnostic performance of dual-energy contrast-enhanced subtracted mammography in dense breasts compared to mammography alone: interobserver blind-reading analysis. Eur Radiol; 24:2394–2403

Christoyianni I, Constantinou E, Dermatas E. (2004). Automatic detection of abnormal tissue in bilateral mammograms using neural networks. Methods Appl Artif Intell.;267–75.

Culliton BJ. (1976). Breast Cancer: second thoughts about routine mammography. Science 193: 555, 1976 .

Dance DR, Thilander KA, Sandborg M, Skinner CL, Castellano IA, Alm G (2000). Influence of anode/filter material and tube potential on contrast, signal-to-noise ratio and average absorbed dose in mammography: a Monte Carlo study. Bri J Radiol, 73: 1056-1067.

De Gelder R, Draisma G, Heijnsdijk EA, et al (2011). Population-based mammography screening below age 50: balancing radiation-induced versus prevented breast cancer deaths. Br J Cancer 2011; 104: 1214–1220.

Del Lama, L.S.; Godeli, J.; Poletti, M.E. Monte Carlo (2017). simulation studies for the determination of microcalcification thickness and glandular ratio through dual-energy mammography. Radiat. Phys. Chem., 137, 157–162.

Del Lama, L.S.; Cunha, D.M.; Poletti, M.E. (2017). Validation of modified PENELOPE Monte Carlo code for applications in digital and dual-energy mammography. Radiat. Phys. Chem, 137, 151–156.

Dhungel N, Carneiro G, Bradley AP. (2017). Fully automated classification of mammograms using deep residual neural networks. In: Biomedical Imaging (ISBI 2017) 2017 IEEE 14th International Symposium on IEEE.. p. 310–4.

Dromain C, Canale S, Saab-Puong S, Carton AK, Muller S, Fallenberg EM. (2014). Optimization of contrast- enhanced spectral mammography depending on clinical indication. J Med Imaging (Bellingham); 1:033506

Duffy SW (2006). Reduction in breast cancer mortality from organized service screening with mammography: further confirmation with external data. Cancer Epidemiol Biomarkers Prev 15:45–51

Enshafi .M et al. (2022). A New method for promote the performance of deep learning paradigm in diagnosing breast cancer: improving role of fusing multiple views of thermography images. Health and Technology Journal.

Fallenberg EM, Dromain C, Diekmann F, et al. (2014). Contrast-enhanced spectral mammography: does mammography provide additional clinical benefits or can some radiation exposure be avoided? Breast Cancer Res Treat 2014; 146:371–381

Fallenberg EM, Dromain C, Diekmann F, et al. (2014). Contrast-enhanced spectral mammography versus MRI: initial results in the detection of breast cancer and assessment of tumour size. Eur Radiol; 24:256–264

Fandos-Morera, A.; Prats-Esteve, M.; Tura-Soteras, J.; Traveria-Cros, A. (1988). Breast tumors: Composition of microcalcifications. Radiology 1988, 169, 325–327.

Fonseca P, Mendoza J, Wainer J, Ferrer J, Pinto J, Guerrero J, et al. (2015). Automatic breast density classification using a convolutional neural network architecture search procedure. In: Proc of SPIE Vol;. p. 941428–1.

Final reports of National Cancer Institute Ad Hoc working groups on Mammography Screening for Breast Cancer and a summary report of their findings and recommendations. Department of Health, Education and Welfare Publication N(NIH)77-1400, Washington D.C. , Government Printing Office, 1977.

Gallego-Posada J, Montoya-Zapata D, Quintero-Montoya O. Detection and Diagnosis of Breast Tumors using Deep Convolutional Neural Networks.

Geras KJ, Wolfson S, Kim S, Moy L, Cho K. (2017). High-Resolution Breast Cancer Screening with Multi-View Deep Convolutional Neural Networks.. arXiv preprint arXiv:170307047.

Greenspan H, van Ginneken B, Summers RM. (2016). Guest editorial deep learning in medical imaging: Overview and future promise of an exciting new technique. IEEE Trans Med Imaging.;35(5):1153–9.

Haas BM, Kalra V, Geisel J, Raghu M, Durand M, Philpotts LE. (2013). Comparison of tomosynthesis plus digital mammography and digital mammography alone for breast cancer screening. Radiology; 269:694–700

Han, Y.; Sun, B.; Yan, H.; Tucker, M.E.; Zhao, Y.; Zhou, J.; Zhao, Y.; Zhao, H. (2020). Biomineralization of Carbonate Minerals Induced by The Moderate Halophile Staphylococcus Warneri YXY2. Crystals 2020, 10, 58.

Hedjazi MA, Kourbane I, Genc Y. On identifying leaves: A comparison of CNN with classical M Lmethods. In: Signal Processing and Communications

Heywang-Köbrunner, Sylvia H., Astrid Hacker, and Stefan Sedlacek.(2011). "Advantages and disadvantages of mammography screening." Breast care 6.3 (2011): 199-207.

Heywang-K.brunner SH, Schreer I, Dershaw DD. (1997). Diagnostic Breast Imaging: Mammography, sonography, magnetic resonance imaging, and intervertional procedures. New York, Georg Thieme Verlag.

Hammerstein GR, Miller DW, White DR, Masterson ME, Woodard HQ, Laughlin JS. (1979). Absorbed radiation dose in mammography. Radiology. 130:485–491. [PubMed: 760167]

Huynh BQ, Li H, Giger ML. (2016). Digital mammographic tumor classification using transfer learning from deep convolutional neural networks. J Med Imaging. 2016;3(3):034501–034501.

Hobbs MM, Taylor DB, Buzynski S, Peake RE. (2015). Contrast-enhanced spectral mammography (CESM) and contrast enhanced MRI (CEMRI): patient preferences and tolerance. J Med Imaging Radiat Oncol 2015; 59:300–305.

Holbrook A, Newel MS. (2015). Alternative screening for women with dense breasts: breast-specific gamma imaging (molecular breast imaging). AJR 2015; 204:252–256 Safety guide Vienna.

IAEA. (2010). Radiation Safety of Gamma, Electrons and X-ray Irradiation Facilities. Specifies

Jaffe M.J. and Maidment A.D.A. Diagnostic Radiology Physics: A Handbook for Teachers and Students: Chapter 9 : Mammography.

James J.R. et al. (2017). Breast Radiation Dose With CESM Compared With 2D FFDM and 3D Tomosynthesis Mammography.

Jennings RJ, Eastgate RJ, Siedband ML, Ergun Dl (1981) Optimal X-ray spectra for screen-film mammography. Med Phys, 8: 629-639.

Jeukens CR, Lalji UC, Meijer E, et al. (2014). Radiation exposure of contrast-enhanced spectral mammography compared with full-field digital mammography. Invest Radiol; 49:659–665.

Jiang F, Liu H, Yu S, Xie Y. (2017). Breast mass lesion classification in mammograms by transfer learning. In: Proceedings of the 5th International Conference on Bioinformatics and Computational Biology. ACM;. p. 59–62.

Jochelson MS, Dershaw DD, Sung JS, et al. (2013). Bilateral contrast-enhanced dual-energy digital mammography: feasibility and comparison with conventional digital mammography and MR imaging in women with known breast carcinoma. Radiology; 266:743–751

Kallenberg M, Petersen K, Nielsen M, Ng AY, Diao P, Igel C, et al. (2016). Unsupervised deep learning applied to breast density segmentation and mammographic risk scoring. IEEE Trans Med Imaging.;35(5): 1322–31.

Kahles A. et al. Big Data Takes on Cancer. Dana-Farber Cancer Institute Advertorial.

Khalkhali, I., Mena, I., & Diggles, L. (1994). Review of imaging techniques for the diagnosis of breast cancer: a new role of prone scintimammography using technetium-99m sestamibi. European journal of nuclear medicine, 21(4), 357-362.

Kooi T, Ginneken B, Karssemeijer N, Heeten A. (2017). Discriminating solitary cysts from soft tissue lesions in mammography using a pretrained deep convolutional neural network. Medical physics.;44(3):1017–27.

Kolb TM, Lichy J, Newhouse JH. (2002). Comparison of the performance of screening mammography, physical examination, and breast US and evaluation of factors that influence them: an analysis of 27,825 patient evaluations. Radiology.;225(1):165–175.

Kooi T, Gubern-Merida A, Mordang JJ, Mann R, Pijnappel R, Schuur K, et al. (2016). A comparison between a deep convolutional neuralnetwork and radiologists for classifying regions of interest in mammography. In: International Workshop on Digital Mammography. Springer; 2016. p. 51–6.

Koukou, V.; Martini, N.; Michail, C.; Sotiropoulou, P.; Fountzoula, C.; Kalyvas, N.; Kandarakis, I.; Nikiforidis, G.; Fountos, G. (2015). Dual Energy Method for Breast Imaging: A Simulation Study. Comput. Math. Methods Med. 574238.

Koukou, V.; Martini, N.; Fountos, G.; Michail, C.; Sotiropoulou, P.; Bakas, A.; Kalyvas, N.; Kandarakis, I.; Speller, R.; Nikiforidis, G. (2017). Dual energy subtraction method for breast calcification imaging. Nucl. Instrum. Methods Phys. Res. A, 848, 31–38.

Koukou, V.; Martini, N.; Fountos, G.; Michail, C.; Bakas, A.; Oikonomou, G.; Kandarakis, I.; Nikiforidis, G. (2017). Application of a dual energy X-ray imaging method on breast specimen. Results Phys., 7, 1634–1636.

Krizhevsky A, Sutskever I, Hinton GE. (2012). Imagenet classification with deep convolutional neural networks. In: Advances in neural information processing systems; 2012. p. 1097–105.

LeCun Y, Bengio Y, Hinton G. (2015). Deep learning. Nature.521(7553):436 44.

Lee JG, Jun S, Cho YW, Lee H, Kim GB, Seo JB, et al. (2017). Deep Learning in Medical Imaging: General Overview. Korean J Radiol.;4(18):570–84.

Lemacks, M.R.; Kappadath, S.C.; Shaw, C.C.; Liu, X.; Whitman, G.J. (2002). A dual-energy subtraction technique for microcalcification imaging in digital mammography—A signal-to-noise analysis. Med. Phys., 29, 1739–1751.

Lester L.G (1977). Risks versus benefit in mammography, Radiology 124: 1-6, 1977.

Levy D, Jain A. (2016). Breastmass classification from mammograms using deep convolutional neural networks. arXiv preprint. arXiv:161200542.

Li H, Giger ML, Huynh BQ, Antropova NO. (2017). Deep learning in breast cancer risk assessment: evaluation of convolutional neural networks on a clinical dataset of full-field digital mammograms. J Med Imaging.;4(4):041304.

Li Y, Chen H, Cao L, Ma J. (2016). A survey of computer-aided detection of breast cancer with mammography. J Health Med Inf.;4(7).

Litjens G, Kooi T, Bejnordi BE, Setio AAA, Ciompi F, Ghafoorian M, et al. (2017). A survey on deep learning in medical image analysis. arXiv preprint arXiv:170205747.

Luczyńska E, Heinze-Paluchowska S, Hendrick E, et al. (2015). Comparison between breast MRI and contrast-enhanced spectral mammography. Med Sci Monit; 21:1358–1367

Mandelson MT, Oestreicher N, Porter PL, et al.(2000). Breast density as a predictor of mammographic detection: comparison of interval- and screen-detected cancers. J Natl Cancer Inst.;92(13): 1081–1087.

Mahmood T, et al. (2020). A Brief Survey on Breast Cancer Diagnostic with Deep Learning Schemes Using Multi-Image Modalities. Journals & Magazines. 2020;8:165779–809.

Martini, N.; Koukou, V.; Fountos, G.; Michail, C.; Bakas, A.; Kandarakis, I.; Speller, R.; Nikiforidis, G. (2017). Characterization of breast calcification types using dual energy X-ray method. Phys. Med. Biol., 62, 7741–7764.

Martini. N et al. (2020). Dual Energy X-ray Methods for the Characterization,Quantification and Imaging of Calcification Minerals and Masses in Breast. MDPI Journals Crystal. 2020.

Mashekova A, et al. (2022). Early detection of the breast cancer using infrared technology – A comprehensive review. Therm Sci Eng Prog.;27.

MK. (2015). Molecular breast imaging: an emerging modality for breast cancer screening. Breast Cancer Manag; 4:33–40

Mohamed AA, Berg WA, Peng H, Luo Y, Jankowitz RC, Wu S. (2017). A deep learning method for classifying mammographic breast density categories. Med Phys.

Mori M, Akashi-Tanaka S, Suzuki S, et al. (2016). Diagnostic accuracy of contrast-enhanced spectral mammography in comparison to conventional full-field digital mammography in a population of women with dense breasts. Breast Cancer 2016 Mar 4

Mowlavi A.A. (2005). X-ray spectra calculation for different target-filter of mammograms using MCNP Code. Iran.

Otto SJ, Fracheboud J, Looman CW et al. (2003). Initiation of population-based mammography screening in Dutch municipalities and effect on breast cancer mortality: a systematic review. Lancet 361:411–417

Oustimov A, Gastounioti A, Hsieh MK, Pantalone L, Conant EF, Kontos D. (2017). Convolutional neural network approach for enhanced capture of breast parenchymal complexity patterns associated with breast cancer risk. In: SPIE Medical Imaging. International Society for Optics and Photonics;. p. 101340S–101340S.

Petersen K, Nielsen M, Diao P, Karssemeijer N, Lillholm M. (2014). Breast tissue segmentation and mammographic risk scoring using deep learning. In: International Workshop on Digital Mammography. Springer; 2014. p. 88–94.

Qiu Y, Wang Y, Yan S, Tan M, Cheng S, Liu H, et al. (2016). An initial investigation on developing a new method to predict short-term breast cancer risk based on deep learning technology. In: SPIE Medical Imaging. International Society for Optics and Photonics.. p. 978521.

Platania R, Shams S, Yang S, Zhang J, Lee K, Park SJ. (2017). Automated Breast Cancer Diagnosis Using Deep Learning and Region of Interest Detection (BC-DROID). In: Proceedings of the 8th ACM International Conference on Bioinformatics, Computational Biology and Health Informatics. ACM;. p. 536–43.

Pisano ED, Gatsonis C, Hendrick E, et al. (2005). Diagnostic performance of digital versus film mammography for breast-cancer screening. N Engl J Med; 353:1773–1783

R.Ramani, N.Suthanthira Vanitha (2014). ,"Computer Aided Detection of Tumours in Mammograms", IJIGSP, vol.6, no.4, pp.54-59,.DOI: 10.5815/ijigsp.2014.04.07.

Rosenberg RD, Hunt WC, Williamson MR et al. (1998). Effect of age, breast density, ethnicity and estrogen replacement therapy on screening mammographic sensitivity and cancer stage at diagnosis: review of 183, 134 screening mammograms in Albuquerque. New Mexico Radiol 209:511– 518

Rashid A.M et al. (2021). Estimating Absorbed Dose to Breast Adipose Tissue from Mammograms. Texas, USA.

Saeed M.K. (2021). Radiation doses and potential cancer risks during mammography procedures at southern Saudi Arabia. International Journal of Radiation Research.

Samala RK, Chan HP, Hadjiiski LM, Helvie MA, Cha KH. Richter CD. (2017). Multi-task transfer learning deep convolutional neural network: application to computer-aided diagnosis of breast cancer on mammograms. Phys Med Biol.;23(62):8894.

Schapira DV, Clark RA, Wolff PA, Jarrett AR, Kumar NB, Aziz NM. (1994). Visceral obesity and breast cancer risk. Cancer;74:632-9.

Shen L. (2017). End-to-end Training for Whole Image Breast Cancer Diagnosis using An All Convolutional Design. arXiv preprint. arXiv:170809427

Shields, M. and Wilkins, K. (2009). An update on mammography use in Canada. Statistics Canada Health Reports. Statistics Canada, Ottawa.

Shuster A, Patlas M, Pinthus JH, Mourtzakis M. (2012). The clinical importance of visceral adiposity: A critical review of methods for visceral adipose tissue analysis. Br J Radiol;85:1-10.

So A. et al. (2020). The Applied Artificial Intelligence Workshop. Packt

Stomper PC, D'Souza DJ, DiNitto PA, Arredondo MA.(1996). Analysis of parenchymal density on mammograms in 1353 women 25–79 years old. AJR Am J Roentgenol.;167(5):1261–1265.

Sun W, Tseng TLB, Zheng B, Qian W. (2016). A preliminary study on breast cancer risk analysis using deep neural network. In: International Workshop on Digital Mammography. Springer;. p. 385–91.

Sutton D (1998) A Textbook of Radiology and Imaging. Churchill Livingstone, London.

Suzuki S, Zhang X, Homma N, Ichiji K, Sugita N, Kawasumi Y, et al. (2016). Mass detection using deep convolutional neural network for mammographic computer-aided diagnosis. In: Society of Instrument and Control Engineers of Japan (SICE) 2016 55th Annual Conference of the. IEEE;. p. 1382–6.

Swamynathan M. (2017). Mastering Machine learning with Python in Six Steps. Apress.

Tabar L, Yen MF, Vitak B et al (2003). Mammography service screening and mortality in breast cancer patients: 20 years follow-up before and after introduction of screening. Lancet 361:1405–1410

Taibi, A.; Vecchio, S. (2014). Breast Imaging. In Comprehensive Biomedical Physics; Elsevier: Amsterdam, The Netherlands; Volume 2, pp. 121–154.

Thibault F, Balleyguier C, Tardivon A, Dromain C. (2012). Contrast enhanced spectral mammography: better than MRI? Eur J Radiol 012; 81(suppl 1):S162–S164

Thilander KA, Ackerholm P, Berlin I, Bjurstam N, Mattsson S et al. (1997). Influence of anode-filter combinations on image quality and radiation dose in 965 women undergoing mammography. Radiology, 203: 348-354.

Valentin J. (1977). The 2007 recommendations of the international commission or radiological protection. Publication;103:53-9.

Yi D, Sawyer RL, Cohn III D, Dunnmon J, Lam C, Xiao X, et al. (2017). Optimizing and Visualizing Deep Learning for Benign/Malignant Classification in Breast Tumors. arXiv preprint arXiv:170506362.

Wang J, Ding H, Azamian F, Zhou B, Iribarren C, Molloi S, et al. (2017). Detecting cardiovascular disease from mammograms with deep learning. IEEE Trans Med Imaging. 2017.

Weiss K, Khoshgoftaar TM, Wang D. (2016). A survey of transfer learning. J Big Data.;3(1):9.

Wrixon AD (2008). New ICRP recommendations. J Radiol Prot; 28: 161–168.

Wu, S.; Chiang, C.Y.; Zhou, W. (2017). Formation Mechanism of CaCO3 Spherulites in the Myostracum Layer of Limpet Shells. Crystals, 7, 319.

Xi P, Shu C, Goubran R. (2018). Abnormality Detection in Mammography using Deep Convolutional Neural Networks.. arXiv preprint. arXiv:180301906.

Xi P, Shu C, Goubran R. (2018). Abnormality Detection in Mammography using Deep Convolutional Neural Networks. 018. arXiv preprint. arXiv:180301906

Zhang X, Zhang Y, Han EY, Jacobs N, Han Q, Wang X, et al. (2017). Whole mammogram image classification with convolutional neural networks. In: Bioinformatics and Biomedicine (BIBM) 2017 IEEE International Conference on. IEEE;. p. 700–4.

Zhao R, Yan R, Chen Z, Mao K, Wang P, Gao RX. (2016). Deep Learning and Its Applications to Machine Health Monitoring: A Survey.. arXiv preprint arXiv:161207640.

Zhu W, Lou Q, Vang YS, Xie X. (2017). Deep multi-instance networks with sparse label assignment for whole mammogram classification. In: International Conference on Medical Image Computing and Computer-Assisted Intervention. Springer;. p. 603–11.